



# Site-specific to local-scale shallow landslides triggering zones assessment using TRIGRS

M. Bordoni<sup>1</sup>, C. Meisina<sup>1</sup>, R. Valentino<sup>2</sup>, M. Bittelli<sup>3</sup>, and S. Chersich<sup>1</sup>

<sup>1</sup>Department of Earth and Environmental Sciences, University of Pavia, Via Ferrata 1, 27100 Pavia, Italy

<sup>2</sup>Department of Civil and Environmental Engineering and Architecture, University of Parma, Viale G. P. Usberti 181/A, 43100 Parma, Italy

<sup>3</sup>Department of Agricultural Sciences, University of Bologna, Viale Fanin 44, 40127 Bologna, Italy

Correspondence to: M. Bordoni (massimiliano.bordoni01@universitadipavia.it)

Received: 24 November 2014 – Published in Nat. Hazards Earth Syst. Sci. Discuss.: 11 December 2014

Revised: 19 March 2015 – Accepted: 4 May 2015 – Published: 21 May 2015

**Abstract.** Rainfall-induced shallow landslides are common phenomena in many parts of the world, affecting cultivation and infrastructure and sometimes causing human losses. Assessing the triggering zones of shallow landslides is fundamental for land planning at different scales. This work defines a reliable methodology to extend a slope stability analysis from the site-specific to local scale by using a well-established physically based model (TRIGRS-unsaturated). The model is initially applied to a sample slope and then to the surrounding 13.4 km<sup>2</sup> area in Oltrepò Pavese (northern Italy). To obtain more reliable input data for the model, long-term hydro-meteorological monitoring has been carried out at the sample slope, which has been assumed to be representative of the study area. Field measurements identified the triggering mechanism of shallow failures and were used to verify the reliability of the model to obtain pore water pressure trends consistent with those measured during the monitoring activity. In this way, more reliable trends have been modelled for past landslide events, such as the April 2009 event that was assumed as a benchmark. The assessment of shallow landslide triggering zones obtained using TRIGRS-unsaturated for the benchmark event appears good for both the monitored slope and the whole study area, with better results when a pedological instead of geological zoning is considered at the regional scale. The sensitivity analyses of the influence of the soil input data show that the mean values of the soil properties give the best results in terms of the ratio between the true positive and false positive rates. The scheme followed in this work allows us to obtain better results in the assessment of shallow landslide triggering areas

in terms of the reduction in the overestimation of unstable zones with respect to other distributed models applied in the past.

## 1 Introduction

Shallow landslides can be defined as slope movements affecting a small thickness (generally lower than 2 m) of superficial deposits. The failure surface is often located along the interface between the soil and bedrock or between soil levels with differences in permeability. These movements are very hazardous phenomena: although they generally involve small volumes of soil, they can be densely distributed across territories as a consequence of particularly intense and concentrated rainfalls (Howard et al., 1988; Montrasio and Valentino, 2008). Moreover, these phenomena are very common in slopes close to urbanized areas; for this reason, they can cause significant damage to cultivation, structures and infrastructures and sometimes cause human losses.

In this work, a methodology that links long-term field observations on a sample slope with a distributed slope stability analysis at the local scale is presented. To assess the occurrence of rainfall-induced shallow landslides in a certain area, three main aspects can be considered to be of prominent importance: (1) a detailed description of the physical–mechanical triggering mechanism in relation to the site-specific characteristics of the involved soils and stratigraphy; (2) the choice of the more suited slope stability model to be applied at the local scale; and (3) the definition of a reliable

methodology to extend the model from the site-specific to local scale, according to the definition of the scale of the analysis proposed by Corominas et al. (2014).

Regarding the first aspect, it is well known that shallow landslide triggering mechanisms are strictly linked to rainfall events with the hydrological and mechanical responses of an usually unsaturated soil. In particular, the quick decrease in negative pore water pressure and the development of positive pressures when a soil approaches saturated conditions could be considered the most important cause of shallow landslides (Lim et al., 1996; Vanapalli et al., 1996). From this perspective, continuously monitoring the climatic and meteorological parameters and the physical and hydrological properties of the unsaturated soil zone is needed to understand the triggering mechanisms of shallow landslides and the main features of these phenomena.

More recently, monitoring techniques have focused not only on the soil's hydrological and mechanical conditions during shallow landslide triggering but also on some unsaturated soil behaviours which could play a primary role in promoting or inhibiting the development of shallow failures. Hydrological monitoring can identify both the predisposing and triggering mechanisms of shallow landslides. Matsushi et al. (2006) analysed rainwater infiltration and groundwater fluxes towards underlying permeable bedrock, which leads to the development of shallow landslides. Some works identified the time changes of the hydrological features of unsaturated soils, which then provoked the triggering of shallow landslides (Matsushi and Matsukura, 2007; Godt et al., 2009; Damiano et al., 2012; Springman et al., 2013). In particular, Godt et al. (2009) were the first to observe the development of a shallow soil failure in unsaturated conditions linked to a rainfall event in a natural setting. Moreover, monitoring systems measured the increase in pore water pressure and the development of a perched water table in the covering soils that could promote shallow landslides (Lim et al., 1996; Godt et al., 2008a, b; Baum et al., 2010, 2011).

The choice of the more suited method to describe the phenomena at the site-specific scale depends on the objectives of the analysis: finite elements methods, for example, can be considered appropriate to analyse an area some hundreds of square metres wide, but they cannot be considered suitable for application at the local or regional scale.

Recently, physically based models proved rather promising in assessing the triggering zones of shallow landslides. Different types of models were developed to analyse the triggering times and locations of shallow landslides according to the following aspects: the development of positive pore water pressures in saturated soils (Montgomery and Dietrich, 1994; Baum et al., 2002), the change in the soil's pore water pressure (Baum et al., 2008; Rossi et al., 2013) or soil saturation (Montrasio and Valentino, 2008) linked to rainfall intensity and duration; the possibility of modelling the size and depth of shallow landslides at the basin and local scale (Alvioli et al., 2014), the connections between different points of a slope

or a basin that influence the soil's hydrological behaviour and the development of unstable conditions (Lanni et al., 2012), and the possibility of modelling the triggering conditions of shallow failures based on the natural variability of geotechnical and hydrological soil features through a probabilistic approach (Grelle et al., 2014; Mergili et al., 2014; Raia et al., 2014). Furthermore, physically based models were used to determine the rainfall thresholds for the timing and localization of shallow landslides at the local and regional scale (Salciarini et al., 2006, 2008; Godt et al., 2008a, b; Papa et al., 2013).

At the moment, an important challenge is represented by the possibility of applying a slope stability model at different scales, keeping the same level of reliability both on single slopes and areas some square kilometres wide. The spatial distribution of both geotechnical and hydrological soil properties can be reasonably inferred only from a limited number of field or laboratory tests, taking into account the spatial variability of the parameters through a probabilistic approach (Simoni et al., 2008; Mergili et al., 2014; Raia et al., 2014).

The implementation of physically based models at the local or regional scale with respect to a single slope requires homogenized soil parameters as input data in the mapping of distinct soil units, the boundaries of which can be defined in different ways. In most cases, the units used in distributed slope stability analyses are defined according to the geology of the bedrock (Salciarini et al., 2006; Baum et al., 2010; Sorbino et al., 2010; Rossi et al., 2013; Park et al., 2013; Zizioli et al., 2013). This choice is linked to the hypothesis that geotechnical and hydrological properties have spatial variations due to the spatial distribution of the bedrock materials from which the soils are derived. More rarely, the mapping unit of the soils is considered according to a pedological classification of the soil deposits (Meisina and Scarabelli, 2007), or these units are defined as engineering–geological or litho-technical units based on the main geotechnical and mechanical properties of the soils in an independent way with respect to the geology of the bedrock (Meisina, 2006; Grelle et al., 2014).

The TRIGRS-unsaturated model (Baum et al., 2008) was applied to a study area in the Oltrepò Pavese (northern Italy; Fig. 1) to assess the triggering zones of shallow landslides, referring to a well-documented case that occurred on 27–28 April 2009 (Zizioli et al., 2013). The main goals of the work were as follows: (i) identify the hydrological behaviour of the slope soils in the study area through continuous field monitoring on a sample slope; (ii) use field data to calibrate the TRIGRS-unsaturated model; (iii) evaluate the efficiency of the TRIGRS-unsaturated model on the estimation of the pore water pressure trend at the site-specific scale; and (iv) compare the results of the TRIGRS-unsaturated distributed analyses at the local scale in the study area, taking into account different mapping units of the slope soils. According to the classification proposed by Corominas et al. (2014), the analyses of the sample slope have been de-

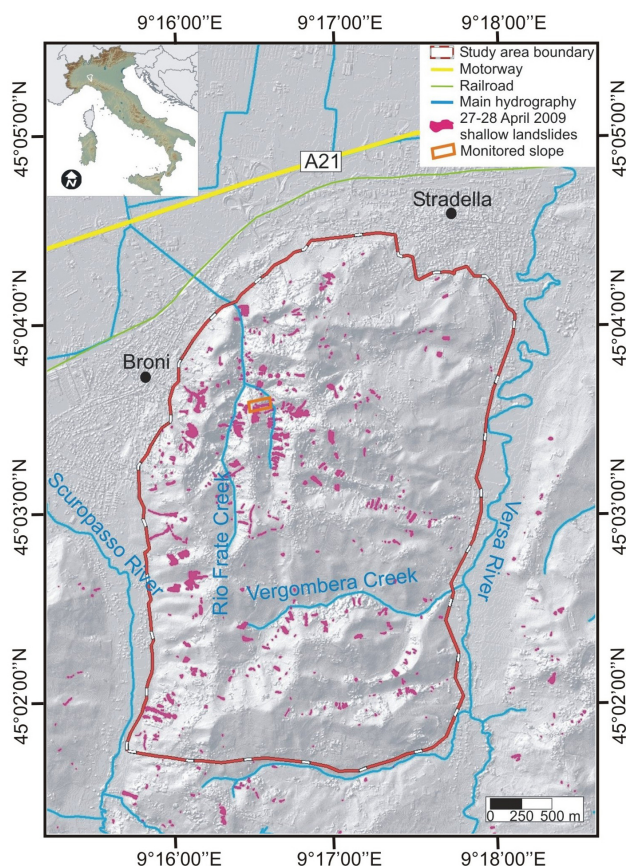


**Figure 1.** Location of the study area.

fined as site-specific because the extent of the sample slope is less than  $10 \text{ km}^2$ , while distributed analyses over the entire study area have been defined as local because the extended area is greater than  $10 \text{ km}^2$ .

In this way, a methodology linking long-term field observations at the site-specific scale with a distributed slope stability analysis at the local scale has been developed.

The study area is strongly characterized by a traditional viticulture, which represents the most important branch of the local economy, and most shallow failures affect slopes cultivated with vineyards. For this reason, it is fundamental to assess the triggering zones of shallow landslides to correctly plan land use, manage agricultural practices and reduce the economic effects of these landslides. The developed methodology may then be applied in other geological contexts where vineyards are located on slopes affected by shallow landslides (Tiranti and Rabuffetti, 2010; Galve et al., 2015).

## 2 The study area

The study area is located in the north-eastern sector of Oltrepò Pavese, which belongs to the north-western Italian Apennines (Fig. 1). The area is  $13.4 \text{ km}^2$  wide and is characterized by the presence of vineyards which constitute 55 % of the land cover, shrub-lands (30 %) and woodlands (15 %) that correspond to vineyards abandoned after the 1980s.

The slopes are characterized by a medium–high gradient with a slope angle that can reach  $35^\circ$  and sometimes descend to small narrow valleys formed by creeks. The slope elevation ranges from 85 to 350 m a.s.l. (above sea level).

The climatic regime is temperate/mesothermal according to Köppen's classification of world climates, with a mean annual temperature of  $12^\circ\text{C}$ . Considering recent rainfall data available from 2004 to 2014 coming from a weather station located near the study area at a similar elevation (Canevino rain-gauge station, ARPA Lombardia monitoring network), the mean yearly rainfall for the period 2004–2014 was 684.4 mm, with the rainfall distributed in fewer but more intense events (Alpert et al., 2002), thus favouring slope instability, as already observed in other environmental contexts (Schnellmann et al., 2010).

In this area, the bedrock is characterized by a series of formations belonging to the Mio–Pliocenic succession that geologically characterizes this Apennine area and is called “Serie del Margine” (Vercesi and Scagni, 1984). Medium–low permeability arenaceous conglomeratic bedrock (Monte Arzolo Sandstones, M. A. Sand.; Rocca Ticozzi Conglomerates, R. T. Cong.) overlies impermeable silty-sandy marly bedrock and evaporitic chalky marls and gypsum (Sant’Agata Fossili Marls, S. F. Marls; Gessoso–Solifera Formation, G. F. Form.) (Fig. 2a). The strata are sub-horizontal, dipping east-north-east. The medium–low hydraulic conductivity of the arenaceous–conglomeratic bedrock is linked to its low primary porosity and the limited number of fractures, which cannot cause the development of a high secondary hydraulic conductivity. The deep water circulation is then confined in less cemented or more fractured levels located at different depths in the bedrock and corresponding to horizons of poorly cemented gravels, sands or conglomerates with a limited lateral extension and thickness ranging between 0.2 and 1.0 m. These bodies do not seem to constitute a continuous, more permeable level that can form a deep aquifer. The presence of water in the bedrock can be identified only by considering the more permeable levels as isolated bodies.

Moreover, a limited number of springs are detected in the valley bottom from the contact between the arenaceous conglomeratic bedrock and sandy-silty marls. These springs are detected only during more rainy periods.

In this sector of the Oltrepò Pavese, the shallow soils are mainly derived from bedrock weathering and have a prevalently clayey-silty or silty-sandy texture. The soil thickness, determined in different points of this area through trench and

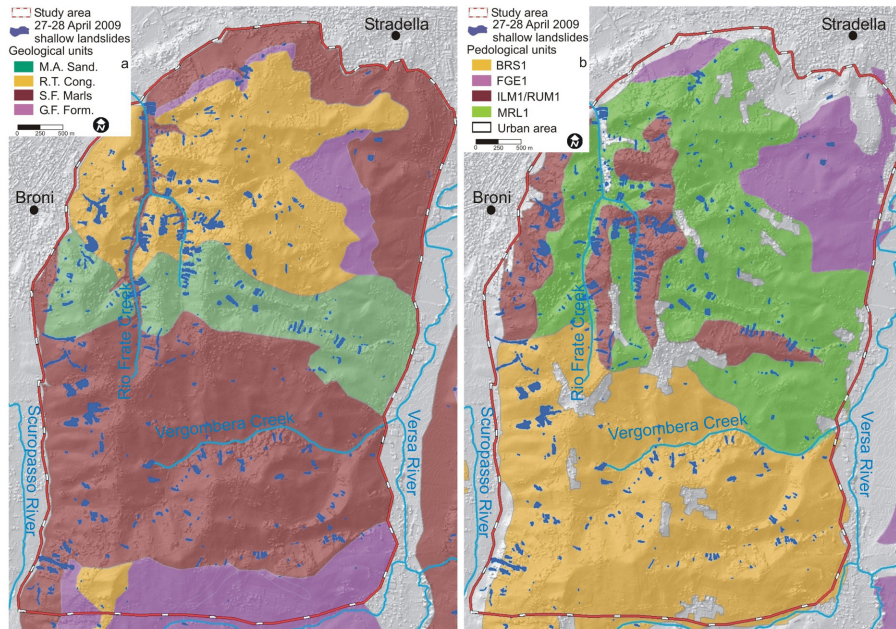


**Figure 2.** Geological (a) and pedological (b) unit distribution across the study area.

manual pits (Zizioli et al., 2013), ranges from a few centimetres to 2.5 m and generally increases from the top to the bottom of the slopes due to the presence of landslide accumulation areas.

The soils have also been classified from a pedological point of view, and this information is available from soil maps at a scale of 1 : 10 000 that cover the entire study area (ERSAL, 2001). Four pedological units can be identified (Fig. 2b):

- BRS1: Eutric Leptosols characterized by good drainage, thickness between 0.3 and more than 2.0 m, high carbonate content (> 20 %) and parent material composed of marls, sandy marls and marly sands;
- FGE1: Calcaric Cambisols characterized by good drainage, thickness that can reach values higher than 1.5 m, high carbonate content (> 20 %) and parent material composed of marls and evaporitic deposits (Gessoso–Solfifera Formation);
- ILM1/RUM1: Eutric Leptosols characterized by good well drainage, thickness lower than 1.5 m, low carbonate content (< 10 %) and parent material composed of sandstones, conglomerates and sandy marls;
- MRL1: Calcaric Cambisol characterized by good drainage, thickness higher than 0.8 m, medium carbonate content (between 10 and 20 %) and parent material composed of sandstone and lenses of conglomerates.

The FGE1 pedological unit seems to be present only where the bedrock consists of deposits from the Gessoso–Solfifera

Formation, while the others are widespread and come from different geological formations.

The study area is characterized by a high density of landslides: the IFFI (Italian Landslides Inventory) database indicates the presence of several deep landslides with failure surfaces below 2–3 m from ground level. In particular, these phenomena are rotational slides, translational slides and complex landslides (roto-translational slides evolving in earth flows) (Cruden and Varnes, 1996) and do not show evidence of recent movement, so they can be classified as dormant landslides. These phenomena were triggered by prolonged rainfall without significantly high intensity.

The widespread shallow landslides that occurred on 27–28 April 2009 constituted the first documented case of a rainfall-induced shallow landslide event to hit the Oltrepò Pavese since the 1950s. Throughout the Oltrepò Pavese area, this event triggered of more than 1600 shallow landslides (Zizioli et al., 2013): the highest density was registered in the study area (491 landslides, approximately 36 landslides per km<sup>2</sup>). Shallow landslides were triggered by an extreme rainfall event characterized by 160 mm of cumulated rain in 62 h with a maximum intensity of 22 mm h<sup>-1</sup> at 21:00 LT on 27 April (Zizioli et al., 2013). This event caused fatalities and damaged or blocked roads in several places (Zizioli et al., 2013).

Additional shallow landslide events occurred in the study area between March and April 2013 (Zizioli et al., 2014) and between 28 February and 2 March 2014. These events triggered a limited number of shallow landslides (17 and 20 respectively) in the study area.

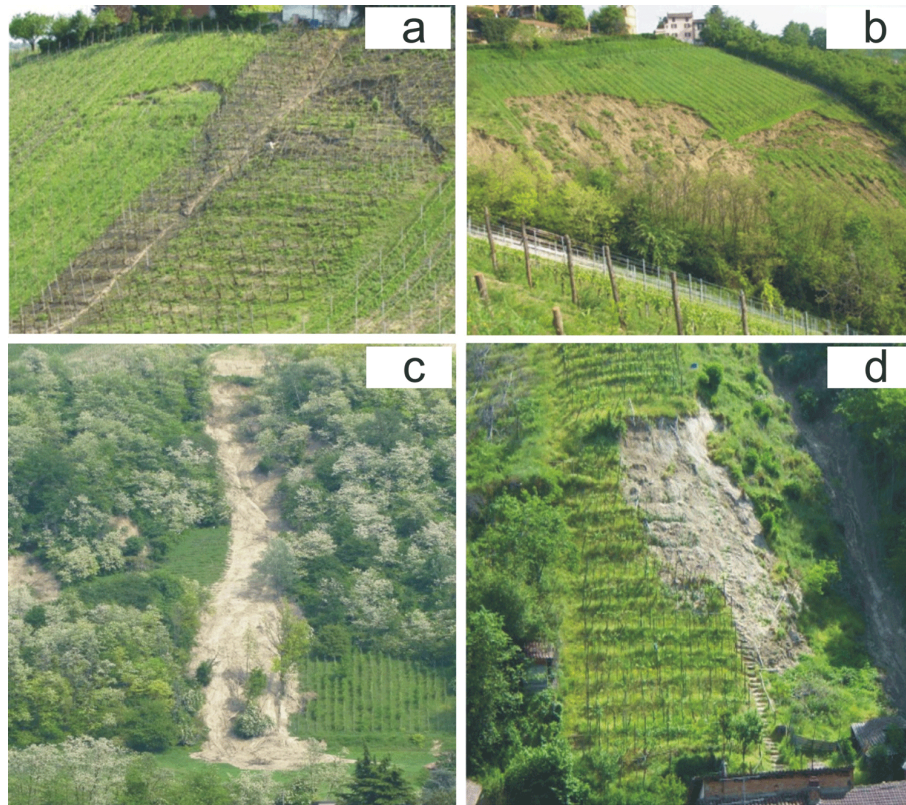


**Figure 3.** Examples of rainfall-induced shallow landslides that occurred in the study area during the event of 27–28 April 2009, according to the classifications of Cruden and Varnes (1996) and Campus et al. (1998): (a) incipient translational slides, (b) translational soil slides, (c) complex landslides and (d) disintegrating soil slips.

The rainfall-induced shallow landslides identified in the study area tended to be concentrated in three main geomorphological contexts: (i) at the top of steep slopes (slope angles  $> 15\text{--}20^\circ$ ) with continuous profiles; (ii) corresponding to a slope angle change from a gentle slope to steep slope; and (iii) in morphological jugs that break the continuity of the slopes. In these areas, the greater superficial runoff and the convergence of sub-superficial outflows in the cover materials promote an increase in the pore water pressure and the saturation of the covering soils. These geomorphological frameworks that promote the development of shallow failure source areas have already been highlighted in other contexts where rainfall-induced shallow landslide events have been triggered (Crosta and Frattini, 2003; D’Amato Avanzi et al., 2004; Dapporto et al., 2005).

According to the classifications of Cruden and Varnes (1996) and Campus et al. (1998) for rainfall-triggered shallow landslides, four main types of landslides were recognized (Fig. 3): (a) incipient translational slides, where fractures are present but the displaced mass has limited movement with little internal deformation (Fig. 3a); (b) translational soil slides, where the mass has moved, the failure surface is completely exposed and the collapsed materials break into different blocks (Fig. 3b); (c) complex

landslides which start as shallow rotational–translational failures and then evolve into earth flows due to the large amount of water and the fabric loss of collapsed materials (Fig. 3c); and (d) disintegrating soil slips, similar to type (c) but in which the accumulation zone is not recognizable because the collapsed materials are completely dispersed along the slope and at its toe (Fig. 3d). Type (c) and type (d) shallow landslides were usually predominant in the events that affected this area.

Shallow landslides mainly affect the superficial soils above weathered or non-weathered bedrock, and the failure surfaces are located along the contact between the soil and bedrock, ranging between 0.5 and 2.0 m from ground level. More rarely, these phenomena have failure surfaces located at the point of contact between soil levels with different permeability. These movements mainly occur in vineyards and uncultivated slopes, where shrubs and grass are prevalent. In contrast, a significant number of landslides involve woodlands formed by trees that had developed in the preceding 30 years on abandoned vineyards.

### 3 Materials and methods

#### 3.1 Soil characterization and monitoring the field hydrological conditions

In the study area, an integrated hydro-meteorological monitoring station was installed on 27 March 2012 in a test-site slope located near the village of Montuè (municipality of Canneto Pavese; Fig. 1).

The slope is characterized by a medium–high topographic gradient (between 22 and 35°), faces the east and descends towards a rather small and narrow valley formed by a creek (Eastern Frate Creek). Its altitude ranges from 210 to 120 m a.s.l. The difference in elevation between the top of the monitored slope and the valley floor is 132 m, while the difference in elevation between the position of the monitoring station and the Rio Frate Creek is 63 m. This slope was chosen as a test-site slope within the study area by considering a series of criteria:

1. the presence of triggering zones of shallow landslides that occurred in April 2009;
2. its position in areas with medium–high susceptibility to shallow landslides according to previous studies (Zizioli et al., 2013);
3. its representativeness of the whole study area in terms of the geomorphological (medium–high topographic gradient) and hydrogeological features (conglomeratic bedrock levels overlying impermeable marly levels);
4. the presence of access roads to easily reach the slope and install instrumentation;
5. its east-facing orientation, allowing for a good recharge of the photovoltaic panel of the station that supplies power to the devices.

A multidisciplinary characterization of the monitored test-site slope was carried out. The representative soil of the slope is 1.3 m thick. The soil belongs to the ILM1/RUM1 pedological unit. Between 1.1 and 1.3 m from the ground, the soil is characterized by the presence of a calcic horizon (C<sub>gk</sub>), labelled as G in Fig. 5, is enriched in carbonate concretions and has a carbonate content of 35.3 %. The soil has a basic pH (approximately 8.3–8.8), a low organic carbon content (less than 3.0 %) and a steady cationic exchange capacity (12.3–15.9 meq L<sup>-1</sup>) along the depth.

The geotechnical characterization of the slope deposits was based on standard soil analyses carried out according to the ASTM (American Society for Testing and Materials) standards. The performed tests included (i) an assessment of the physical parameters of the materials (grain size distribution, bulk density, Atterberg limits) and (ii) triaxial tests which allowed the determination of the shear strength parameters in terms of the effective stresses.

The soil derives from the weathering of sands and poorly cemented conglomerates belonging to the Rocca Ticozzi Conglomerates. Individual soil horizons along the slope have a clayey sandy silt texture, with high silt contents ranging from 51.1 to 65.6 %, clay content between 21.3 and 29.0 % and varying amounts of gravel and sand (Table 1). By analysing the clay soil fraction (< 2 µm) through X-ray diffraction tests, the clay mostly appears to consist of smectite and chlorite. In particular, smectite constitutes approximately 50 % of the finest soil fraction and approximately 10–15 % of the solid particles in the studied soils. The weathered bedrock 1.4 m from the ground, labelled as We. Bed. in Fig. 5, consists of a sand lens with a sand content of 75.0 % (Table 1).

According to the USCS classification, the soil horizons are prevalently non-plastic or slightly plastic (CL). The liquid limit ( $w_L$ ) ranges from 38.5 to 41.9 %, while the plasticity index ( $P_I$ ) ranges from 14.3 to 17.1 %, and both remain steady along the depth (Table 1). The unit weight ( $\gamma$ ) increases between 0.6 and 1.0 m b.g.l. (below the ground level) from 16.7 to 18.6 kN m<sup>-3</sup> and then remains steady with depth (Table 1).

The peak shear strength parameters were reconstructed at different depths through triaxial tests. Up to 1.0 m from the ground, the soil horizons have a friction angle ( $\varphi'$ ) between 31 and 33° and nil effective cohesion ( $c'$ ) (Table 1). At 1.2 m from the ground, the soil level is characterized by a friction angle equal to 26° and effective cohesion of 29 kPa (Table 1).

The hydrological properties of the different soil horizons were determined through a laboratory reconstruction of the soil water characteristic curve (SWCC) and the hydraulic conductivity function (HCF). These functions were reconstructed through a combination of the Wind–Schindler method (WSM; Schindler, 1980; Peters and Durner, 2008) technique (Hyprop, UMS GmbH, Munich, Germany) with a vapour pressure method (VPM; Rawlins and Campbell, 1986) device (WP4T, Decagon Devices, Pullman, WA) on undisturbed soil samples. The experimental data were fitted by the Van Genuchten (1980) and Mualem (1976) models. The parameters of these models (saturated water content  $\theta_s$ , residual water content  $\theta_r$ , fitting parameters  $\alpha$  and  $n$  and saturated hydraulic conductivity  $K_s$ ) were then estimated using the Marquardt (1963) algorithm. All the soil levels had similar values of  $\alpha$  (0.007–0.013 kPa<sup>-1</sup>) and  $\theta_r$  (1–3 %). The  $n$  and  $\theta_s$  parameters were slightly higher until 0.6 m from the ground with respect to the deeper levels. Moreover,  $K_s$  was quite steady at approximately 1.0 and  $2.5 \times 10^{-6}$  m s<sup>-1</sup> except for the soil level at 1.2 m from the ground, which was less permeable ( $0.5 \times 10^{-6}$  m s<sup>-1</sup>; Table 2).

A detailed description of the monitoring station is reported elsewhere (Bordoni et al., 2014; Fig. 4). In this paper, the necessary information required for completeness is provided. The station collects data with a time resolution of 10 min. The following meteorological parameters are measured: rainfall depth, air temperature, air humidity, atmospheric pres-

**Table 1.** Selected geotechnical and mechanical features of the monitored slope soil and weathered bedrock: grain size distribution (gravel, sand, silt, clay), liquid limit ( $w_L$ ), plasticity index ( $P_I$ ), unit weight ( $\gamma$ ), friction angle ( $\phi'$ ), cohesion ( $c'$ ).

Representative depth m	Gravel (%)	Sand (%)	Silt (%)	Clay (%)	$w_L$ (%)	$P_I$ (%)	$\gamma$ ( $\text{kN m}^{-3}$ )	$\phi'$ ( $^\circ$ )	$c'$ (kPa)
0.2	12.3	12.5	53.9	21.3	39.8	17.2	17.0		
0.4	1.5	11.4	59.4	27.7	38.5	14.3	16.7	31	0.0
0.6	8.5	13.2	51.1	27.2	40.3	15.7	16.7	31	0.0
1.0	2.4	12.2	56.4	29.0	39.2	15.9	18.6	33	0.0
1.2	0.5	7.5	65.6	26.4	41.9	16.5	18.3	26	29.0
1.4	0.2	75.0	24.8	0.0	–	–	18.1		

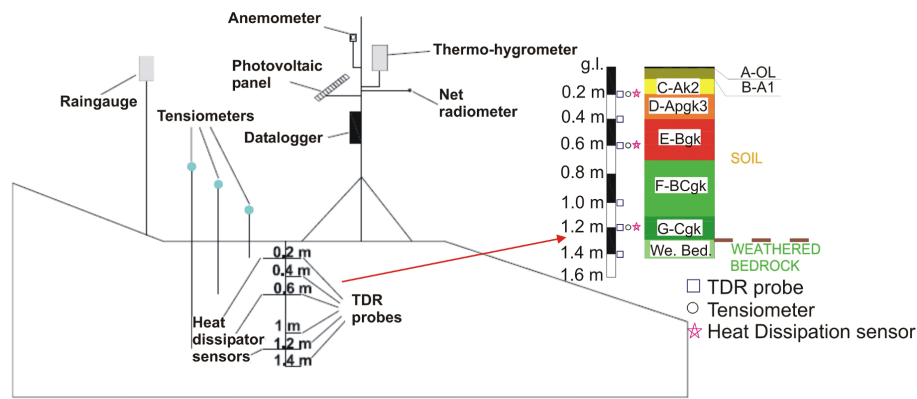


**Figure 4.** Schematic representation of the monitoring station installed in the study area.

**Table 2.** Hydrological properties of the monitored slope soil and weathered bedrock.

Representative depth m	$\alpha$ ( $\text{kPa}^{-1}$ )	$n$ (–)	$\theta_s$ (%)	$\theta_r$ (%)	$K_s$ ( $\text{m s}^{-1}$ )
0.2	0.013	1.43	43	3	$2.5 \times 10^{-6}$
0.4	–	–	–	–	–
0.6	0.010	1.40	42	1	$1.5 \times 10^{-6}$
1.0	0.009	1.38	39	2	$1.0 \times 10^{-6}$
1.2	0.007	1.34	40	1	$0.5 \times 10^{-6}$
1.4	–	–	–	–	–

sure, net solar radiation, wind speed and direction. Some probes are installed in the soil and weathered bedrock at different depths to measure the soil water content and soil pore water pressure. In particular, six time domain reflectometer (TDR) probes installed at 0.2, 0.4, 0.6, 1.0, 1.2 and 1.4 m from the ground level measure the soil water content, while a combination of three tensiometers and three heat dissipation (HD) sensors installed at depths of 0.2, 0.6 and 1.2 m measure the soil’s pore water pressure. The HD sensors only allow pore water pressures lower than  $-10^1$  kPa (Bittelli et al., 2012) to be acquired; thus, tensiometers are installed along-

side the HD sensors to measure pore water pressures above  $-10^1$  kPa.

The monitoring equipment allowed us to identify the soil’s main hydrological behaviours, in particular the soil’s response to the different seasonal rainy conditions and various rainfall intensities. The test-site slope can adequately represent the geotechnical and hydrological features of slopes affected by shallow landslides over the entire study area. For this reason, the data from continuous monitoring of the sample slope can be useful to identify the soil’s hydrological conditions that can lead to the triggering mechanisms of shallow landslides in similar conditions. The field data can be used to infer the soil conditions for periods without monitoring to evaluate the prediction ability of a physically based model such as TRIGRS-unsaturated, which is used to identify the triggering zones of shallow landslides at the local scale.

### 3.2 Homogenization of the soil parameters in the study area

To identify the triggering zones of shallow landslides using physically based models, the distributions of the main geotechnical and hydrological properties are required as input parameters to obtain the trend of the slope safety factor ( $F_s$ ) in time. However, transitioning from the site-specific scale, where detailed field and laboratory test results can be

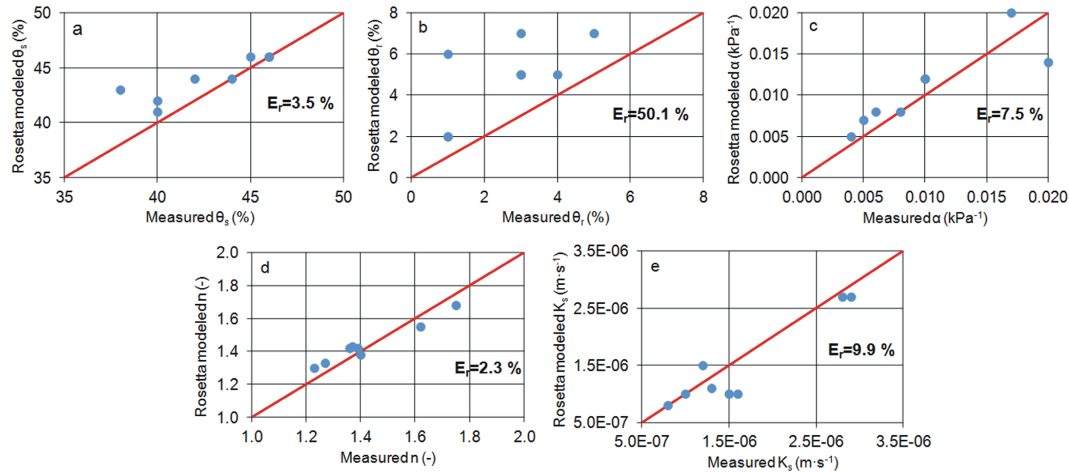


**Figure 5.** Comparison of measured and modelled parameters of Mualem and Van Genuchten models for some soil samples taken in the study area, obtained through Rosetta pedotransfer function: (a)  $\theta_s$ , (b)  $\theta_r$ , (c)  $\alpha$ , (d)  $n$ , (e)  $K_s$ .

available, to a local scale, where data can be available only for a limited number of sites, it is important to establish which characteristics should be considered “constant” to enable the assumption that the available data are representative.

To guess an answer to this question, the TRIGRS model was implemented in the study area using different types of mapping units (geological and pedological), the class distribution of which across the study area is represented in Fig. 3.

The main geotechnical and mechanical soil properties were assigned to each unit after performing an averaging procedure of the data collected through laboratory tests on 160 soil samples taken from different sites in the study area. In this group, 114 disturbed soil samples were used to determine the Atterberg limits and grain size distribution curves, while 52 undisturbed soil samples were used to measure the soil’s unit weight. In the group of undisturbed soil samples, which were taken at a depth where the failure surface of the shallow landslides developed, 18 samples were used to measure the peak shear strength parameters through direct shear tests, and 3 samples were used for triaxial tests. As observed in the monitored slope, no significant changes in the geotechnical properties, particularly for the grain size distribution and Atterberg limits, were identified along the depth in the soil levels.

The main differences between the classes for each mapping unit type were linked to the grain size distribution. In fact, the geological and pedological units could be distinguished based on the sand and clay amounts. The soils derived from the weathering of the Monte Arzolo Sandstones and Rocca Ticozzi Conglomerates were classified as clayey-sandy silt because the amount of sand is generally more than 15 % (Table 3). In contrast, the soils derived from the weathering of the Sant’Agata Fossili Marls and Gessoso–Solifera Formation were classified as clayey silt due to a sand content generally lower than 10 % and a prevalent silt content (Ta-

ble 3). Moreover, the soils derived from the weathering of the Gessoso–Solifera Formation exhibited a significantly higher clay content (37.1 %) than the other units (Table 3). The BRS1 and MRL1 pedological units contain groups of soils with clayey silt texture (Table 3), while the ILM1/RUM1 soils are clayey-sandy silt due to a mean sand content of 19.3 %. In contrast, the FGE1 class contains soils with a clayey-silty texture due to similar mean silt and clay contents (46.9 and 43.3 % respectively; Table 3).

According to the USCS classification, the majority of the classes in all the mapped units are grouped into non-plastic or slightly plastic soils (CL), with a mean liquid limit  $w_L$  that ranges between 39.7 and 43.9 % and a mean plasticity index  $P_I$  that ranges between 18.1 and 22.7 % (Table 3). Only the FGE1 pedological class presents highly plastic soils (CH) with a mean  $w_L$  of 52.4 % and a mean  $P_I$  of 31.8 % (Table 3).

The unit soil weight  $\gamma$  is similar among the different classes for each mapping unit (Tables 1–3); the mean values range between 17.0 and 18.1 kN m<sup>-3</sup>. Furthermore, the shear strength parameters of the soils, i.e. the peak friction angle  $\varphi'$  and the effective cohesion  $c'$ , are quite similar for all the considered soils (Table 3). In particular,  $\varphi'$  ranges between 24 and 27°, while  $c'$  remains between 1.2 and 2.0 kPa.

The standard deviation (SD) value of each soil property for each unit has also been provided. For both geological and pedological units, the highest values of SD were measured for the liquid limit  $w_L$ , the sand and silt content and the shear strength parameters  $\varphi'$  and  $c'$  (Table 3). In particular,  $c'$  reaches SD values on the order of 80–100 % of the mean value (Table 4).

A similar procedure was performed to assign the hydrological parameters (in terms of SWCC) to the different selected units. In particular, the Rosetta pedotransfer function model (Schaap et al., 2001) was applied to the grain size distribution of the soil samples to determine the parameters of the

**Table 3.** Mean and standard deviation (SD) values of geotechnical and mechanical characteristics of the unit mapping of the soils of the study area. The SD values are in parentheses.

	$w_L$ (%)	$P_I$ (%)	Gravel (%)	Sand (%)	Silt (%)	Clay (%)	$\gamma$ ( $\text{kN m}^{-3}$ )	$\varphi'$ ( $^\circ$ )	$c'$ (kPa)
Geological unit									
Monte Arzolo Sandstones (SD)	43.9 (4.5)	22.7 (5.0)	2.4 (3.5)	16.0 (11.6)	55.6 (7.1)	26.0 (8.7)	17.9 (1.2)	26 (4)	1.9 (1.1)
Rocca Ticozzi Conglomerates (SD)	41.2 (4.6)	18.5 (7.4)	5.1 (5.1)	17.9 (12.6)	53.1 (10.1)	23.9 (6.4)	17.7 (1.5)	27 (4)	1.5 (3.5)
Sant'Agata Fossili Marls (SD)	42.0 (13.6)	22.6 (13.1)	1.7 (1.0)	8.3 (4.5)	52.9 (6.4)	37.1 (4.9)	18.0 (1.5)	26 (4)	2.0 (3.0)
Gessoso– Solfifera Formation (SD)	41.9 (11.9)	21.2 (7.1)	2.0 (2.2)	9.1 (4.7)	53.4 (5.4)	29.5 (6.5)	17.8 (0.8)	24 (3)	1.8 (3.0)
Pedological unit									
BRS1 (SD)	42.3 (3.2)	21.3 (2.7)	1.3 (1.0)	10.5 (6.5)	58.2 (4.5)	30.0 (5.9)	17.0 (1.1)	24 (6)	1.2 (1.2)
FGE1 (SD)	52.4 (1.9)	31.8 (1.7)	1.5 (2.0)	8.3 (3.8)	46.9 (3.6)	43.3 (2.3)	17.5 (1.2)	26 (2)	2.0 (3.0)
ILM1/RUM1 (SD)	40.7 (5.1)	18.1 (4.5)	4.8 (5.2)	19.3 (12.6)	52.4 (10.1)	23.5 (7.3)	18.1 (1.2)	26 (4)	1.5 (4.2)
MRL1 (SD)	42.2 (5.1)	21.0 (5.0)	3.3 (3.4)	12.1 (9.2)	56.7 (7.6)	27.9 (7.2)	18.1 (1.5)	25 (3)	1.5 (3.4)

SWCCs and HCFs of the materials of each identified class according to the models of Mualem and Van Genuchten (Table 4). The average values of the Mualem and Van Genuchten models' parameters ( $\theta_s$ ,  $\theta_r$ ,  $\alpha$ ,  $n$ ,  $K_s$ ) are very similar between the classes (Table 4). In contrast, the SD values are quite high, between 20 and 70 % of the mean value (Table 4). The high SD of each mapping unit is linked to the high SD value of the soil fractions (gravel, sand, silt and clay), which are required in the Rosetta model to assess the SWCC properties.

The WRCs and HCFs were also reconstructed for eight undisturbed samples taken in the study area through the same methods (WSM and VPM) used for the soil samples from the monitored slope. For these soils, the reconstructed Mualem and Van Genuchten model parameters are confident with respect to the values modelled through the Rosetta pedotransfer function for  $\theta_s$ ,  $\alpha$ ,  $n$  and  $K_s$ : in fact, the percentage of the mean error ( $E_r$ ) ranges between 2.3 and 9.9 % (Fig. 5a, c, d, e). Only the  $\theta_r$  values modelled through Rosetta are notably higher than the values measured through the Hyprop technique ( $E_r = 50.1$  %, Fig. 5b). Generally, this error is not so

large considering the low values that characterize the studied soil (e.g. measured  $\theta_r$  of 2 % against an estimated  $\theta_r$  of 4 %).

This aspect confirms the reliability of modelling the soil's hydrological properties in the study area through the Rosetta model, correctly identifying the mean values of these properties to be assigned to the selected mapping unit classes.

### 3.3 Shallow landslides triggering zone identification

The TRIGRS-unsaturated model (Baum et al., 2008) has been used for the analyses to assess the triggering zones of shallow landslides in the study area. A brief description of the main principles of this physically based model is provided in Appendix A.

This model has been applied to different rainfall events measured by the monitoring station installed in the study area during its activity. The modelled pore water pressures at two depths, 0.6 and 1.2 m from the ground, for each considered rainfall event along the monitored slope were then compared with the values measured during the same rainfall at the monitoring station. The goodness of the TRIGRS-unsaturated model's fit to the pore water pressure modelling

**Table 4.** Mean and standard deviation (SD) values of hydrological properties of the unit mapping of the soils of the study area. The SD values are in parentheses.

	$\theta_s$ (%)	$\theta_r$ (%)	$\alpha$ (kPa <sup>-1</sup> )	$n$ (–)	$K_s$ (m s <sup>-1</sup> )
Geological unit					
Monte Arzolo Sandstones (SD)	44 (5)	6 (5)	0.006 (0.010)	1.57 (0.32)	$1.5 \times 10^{-6}$ ( $0.5 \times 10^{-6}$ )
Rocca Ticozzi Conglomerates (SD)	43 (7)	5 (4)	0.006 (0.007)	1.58 (0.34)	$1.5 \times 10^{-6}$ ( $0.5 \times 10^{-6}$ )
Sant'Agata Fossili Marls (SD)	46 (5)	8 (6)	0.007 (0.010)	1.54 (0.28)	$1.4 \times 10^{-6}$ ( $0.6 \times 10^{-6}$ )
Gessoso–Solfifera Formation (SD)	48 (4)	8 (7)	0.010 (0.008)	1.46 (0.31)	$1.4 \times 10^{-6}$ ( $0.5 \times 10^{-6}$ )
Pedological unit					
BRS1 (SD)	46 (4)	7 (6)	0.007 (0.006)	1.53 (0.41)	$1.5 \times 10^{-6}$ ( $0.5 \times 10^{-6}$ )
FGE1 (SD)	49 (7)	9 (5)	0.012 (0.07)	1.39 (0.27)	$1.5 \times 10^{-6}$ ( $0.5 \times 10^{-6}$ )
ILM1/RUM1 (SD)	43 (4)	5 (5)	0.006 (0.007)	1.58 (0.34)	$1.4 \times 10^{-6}$ ( $0.5 \times 10^{-6}$ )
MRL1 (SD)	45 (5)	8 (6)	0.007 (0.006)	1.55 (0.32)	$1.4 \times 10^{-6}$ ( $0.5 \times 10^{-6}$ )

was evaluated with the root mean square error (RMSE) statistical index, expressed in Eq. (1) as

$$\text{RMSE} = \sqrt{\frac{\sum_{i=1}^n (\psi_{o,i} - \psi_{m,i})^2}{n}}, \quad (1)$$

where  $\psi_o$  is the observed water pore water pressure at the  $i$ th hour of the considered rainfall events in Tables 7 and 8;  $\psi_m$  is the pore water pressure estimated by the model at the same  $i$ th hour of the same event; and  $n$  is the number of observations, which corresponds to the duration of the rainfall. As the RMSE value approaches 0 kPa, the prediction model becomes increasingly effective and accurate. Only a comparison between the measured and modelled pore water pressure trends at different depths by the monitoring station on the sample slope has been considered.

Moreover, TRIGRS-unsaturated was applied considering the benchmark rainfall event on 27–28 April 2009. Referring to a real rainfall event, these analyses provided the assessment of shallow landslide triggering zones taking into

account the two different types of mapping units, namely geological and pedological. The choice to also consider the pedological unit is linked to the distinction of the soils in the study area based on their pedological features, which can be connected to different pedological processes that can directly influence the physical and hydrological behaviour of a soil (Baumhardt and Lascano, 1993). Two indexes from the receiver operating characteristic analysis (Hosmer and Lemeshow, 2000; Zizioli et al., 2013) have been used to evaluate the predictive capability of the reconstructed models: the “true positive rate” (TP) and the “false positive rate” (FP). The TP is the ratio (in percentage) between the number of elementary cells computed as unstable (safety factor < 1.0) by the model and the number of elementary digital elevation model (DEM) cells occupied by shallow landslide triggering areas. In contrast, the FP represents the ratio (in percentage) between the number of elementary cells computed as unstable that do not correspond to observed shallow landslide triggering zones and the number of elementary cells in the study area not affected by the phenomena and thus considered stable (safety factor > 1.0).

The results of the reconstructions through the TRIGRS-unsaturated model were also compared, in terms of the TP and FP, with the results obtained in a previous work through the TRIGRS-saturated (Baum et al., 2002), SINMAP (Pack et al., 1999) and SLIP (Montrasio and Valentino, 2008) models in the same study area and for the same event by Zizioli et al. (2013).

## 4 Results

### 4.1 Monitored soil and weathered bedrock hydrological behaviours

As reported in the introduction, the first step to appropriately model rainfall-induced landslides at both the site-specific and local scales is a detailed description of the physical–mechanical triggering mechanism in relation to the site-specific characteristics of the involved soils and stratigraphy. Data from the monitoring station were used to determine the dynamics of the soil's water content and soil's pore water pressure at the test site in relation to the characteristics of the different soil levels and the weathered bedrock (Fig. 6). The monitored hydrological behaviours can adequately represent the typical conditions that characterize the surrounding study area. In this work, the period between 27 March 2012 and 1 October 2014 was analysed.

The average hourly values of the water content and pore water pressure were considered. Because the tensiometer at 0.2 m from the ground level broke, the pore water pressure in the range between 0 and  $-10^1$  kPa was not measured at this depth from November 2012 until the end of the analysis period. No data were acquired between 10 and 15 Jan-

uary 2014 because the station's alimentation system did not function correctly.

In the analysis period, the water content ranged between 10 and 45 % in the topsoil and between 15 and 38 % in the weathered bedrock. In contrast, the pore water pressure ranged from positive values to 12.7 kPa in the G horizon to values on the order of  $-10^3$  kPa.

The installed tensiometers required a correction for the measured values due to the height of the water present in the column of the instrument, with an increase of 1 kPa for each 0.1 m of depth in the soil. For this reason, it is possible to measure positive pore water pressure values, as already shown in previous works (Zhan et al., 2006).

By analysing the data acquired over 2 years of monitoring, it is immediately clear that the water content and pore water pressure dynamics are strictly connected to rainfall trends and different hydrological behaviours can be identified in the soil profile (Fig. 6).

The soil horizons within 0.6–0.7 m of ground level had a faster response than the deepest soil horizons to long, dry or long, wet periods. In the summer months, the water content and pore water pressure decreased faster in the most shallow soil horizons than in the deeper ones (Fig. 6) due to evapotranspiration effects and water uptake from the roots of grass and shrubs. Changes in the hydrological parameters are less rapid in soil levels deeper than 0.6–0.7 m below the surface and in weathered bedrock (Fig. 6); this different behaviour is linked to the fact that these levels are less affected by evapotranspiration and root zone effects. The shallowest soil horizons quickly became wet (Fig. 6) during rather prolonged rainy periods following dry periods, such as in autumn months, and after rainfall events characterized by low duration and low cumulative rainfall (e.g. 34.8 mm in 21 h on 31 October–1 November 2012 and 42.2 mm in 34 h on 6–7 October 2013). In contrast, the re-wetting of soil horizons deeper than 0.6–0.7 m below the surface and the weathered bedrock is not so fast, and only prolonged rainy periods with many rainfall events in a few days or weeks can provoke an increase in the pore water pressure and water content at this level (Fig. 6).

The rapid re-wetting as a consequence of early autumn rainfalls of the soil horizons within 0.6–0.7 m and the abrupt increase in pore water pressure in a time span of 5–10 h after the start of the rain during summer concentrated events, as it occurred on 27 June 2013 (13.3 mm in 2 h), on 26 August 2013 (16.5 mm in 3 h) and on 11 September 2013 (9.1 mm in 3 h), may also be due to the presence of desiccation cracks and other macro-voids all along the soil profile where rainwater may flow preferentially. This fact could promote a quick development towards near saturated conditions in the cracks and macro-voids (Bittelli et al., 2012; Smethurst et al., 2012).

In the winter and spring months, especially between December and May, frequent precipitation can increase the soil wetness until it approaches or reaches saturated conditions

(Figs. 6 and 7). The soil water content ranges between 38 and 45 %. In contrast, the pore water pressure remains between  $-7$  and  $-3$  kPa in soil horizons within 0.6 m of the surface, while completely saturated conditions were reached in the G horizon at 1.2 m from ground as testified by the values of pore water pressure which remained quite steady at approximately 0 kPa (Fig. 7) until it reached positive values of approximately 1–3 kPa in response to more intense rainfall events (e.g. 29.8 mm in 24 h on 24–25 March 2013; 24.6 mm in 15 h on 30 March 2013; 29.5 mm in 26 h on 4–5 April 2013; 34.6 mm in 44 h on 18–20 January 2014; 68.9 mm in 42 h on 28 February–2 March 2014). Thus, in this situation, a moderately intense rainfall could not cause a further increase of pore water pressure and water content (Figs. 6 and 7).

During wet periods, the water content in the weathered bedrock at 1.4 m below the surface was lower than in the overlying G horizon (Fig. 6a).

According to the monitored data, it might be hypothesized that during winter and spring months a perched water table can form in the test-site slope soils due to the contact between the soil and weathered bedrock and remain steady at 1.2 m below the surface until the end of the spring. The thickness of this water table is approximately 0.1 m over the contact between the soil and the weathered bedrock. Additionally, when no rain falls for many days, as between 5 and 21 March 2014 (Fig. 7), the pore water pressure remains steady within a positive value range at this depth, thus confirming the presence of a perched water table. In contrast, following particularly intense rainfalls, water table can grow up to 0.8–1.0 m as testified by the significant increase in water content at 1.0 m from ground until conditions of complete saturation are attained (water content between 39 and 42 %).

This condition was not observed following other rainfall events in wetting periods during the monitored time span. In this situation, a shallow landslide affected the test-site slope (Fig. 7). For this reason, the triggering mechanism of rainfall-induced shallow landslides in the study area could be due to the emergence of a thin (0.1–0.2 m) perched water table present in winter and spring months in the slope soils of the study area following particularly intense rainfalls. Thus, it is fundamental to take into account this mechanism on modelling shallow landslides triggering zones through physically based models.

The particular hydrogeological setting of the bedrock levels does not allow for the formation of a deep groundwater level in the slope, but the water table develops only at the interface between soil and weathered bedrock. Other evidence demonstrates the absence of a deep groundwater level. Figure 8 shows the trends of water electrical conductivity measured through the TDR probes of the monitoring station at different depths in soil and weathered bedrock levels. The electrical conductivity values range between 15 and  $40 \mu\text{S cm}^{-1}$  in the soil profile within 1.0 m from ground level, with the highest values following wet periods characterized

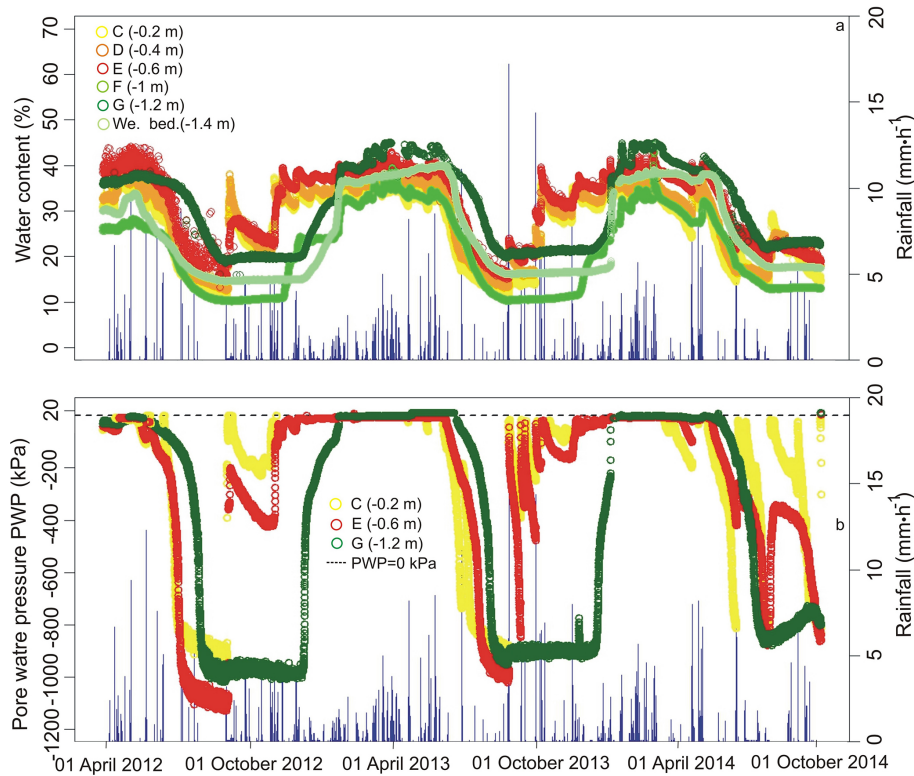


**Figure 6.** Monitored soil and weathered bedrock water content (a) and pore water pressure dynamics (b) at the monitored test-site slope in the study area.

by more frequent rainfalls. In the same periods, the water electrical conductivity reaches values of  $50 \mu\text{S cm}^{-1}$  at 1.2 m from the ground level. The weathered bedrock level at a depth of 1.4 m has values in a similar range with respect to the shallower soil horizons (Fig. 8). According to these data, it seems clear that there is no uprising of a deep water table from the bedrock to the superficial soil, as demonstrated by water electrical conductivity values in the range of rainfall water. Moreover, the highest values measured at a depth of 1.2 m in the G horizon during the winter and spring months suggest the temporary formation of a perched water table at this level, which can arise from more intense rainfall events up to the shallower levels (Fig. 8).

Based on monitoring observations, the development of a thin perched water table above the soil–bedrock contact seems to be the most reasonable hydrological mechanism for shallow landslide triggers in this area, even if other mechanisms (e.g. bedrock exfiltration; Brönnimann et al., 2013) cannot be completely excluded. Moreover, the soil–atmosphere interaction phenomena observed during wet periods were considered a good benchmark for the application of the TRIGRS-unsaturated model. In fact, the model allows for the modelling of shallow landslide triggers due to the emergence of a perched water table (Baum et al., 2008), as we can observe in the monitored test site. This fact implies that the lowest computed safety factors correspond to areas char-

acterized by the presence of a natural permeability barrier, such as the soil-weathered bedrock contact where shallow landslide sliding surfaces develop, as can be observed in the study area (Zizioli et al., 2013).

#### 4.2 TRIGRS-unsaturated model implementation

A DEM acquired before the April 2009 event with a grid size of  $10 \text{ m} \times 10 \text{ m}$  provides the topographic basis for the study area reported in Fig. 1. The TRIGRS-unsaturated model was also applied on the monitored slope with a more detailed DEM, with a grid size of  $2 \text{ m} \times 2 \text{ m}$  over an area of approximately  $3290 \text{ m}^2$ .

TRIGRS-unsaturated was implemented with both DEMs to evaluate the differences in the models when passing from the site-specific scale and high resolution to a local scale with lower resolution.

To analyse the role played by the types of mapping units, the study area was divided into different regions according to each zoning. All input data were acquired from a GIS database in a “raster” form. For each mapping unit, a map was generated at the same spatial resolution as the DEM.

The soil’s geotechnical and hydrological parameters are required as input data by TRIGRS-unsaturated and are summarized in Table 5. To take into account the uncertainties of the soil input data, the triggering zones of the shallow land-

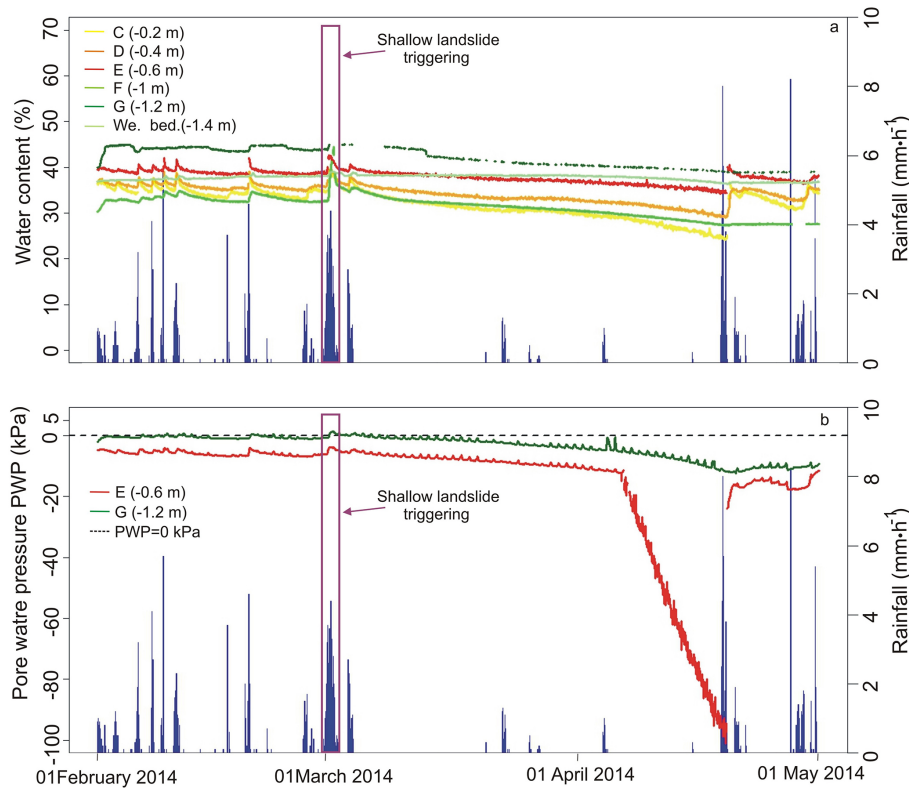


**Figure 7.** Monitored soil and weathered bedrock water content (a) and pore water pressure dynamics (b) at the monitored test-site slope between 1 February and 1 May 2014.

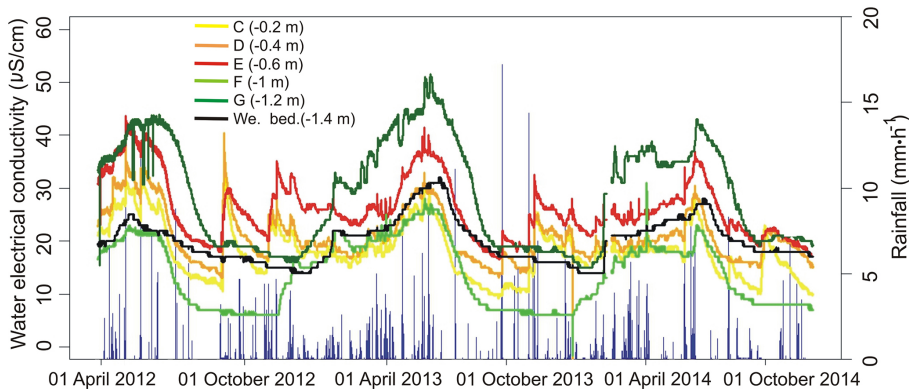


**Figure 8.** Monitored soil and weathered bedrock water electrical conductivity dynamics at the monitored test-site slope in the study area.

slides were modelled by considering either the mean value or the value obtained by subtracting or adding the standard deviation of each parameter. A sensitivity analysis was performed through different simulations by changing only one parameter in each simulation and keeping the others constant. The considered variables were the unit weight  $\gamma$ , the peak friction angle  $\phi'$ , the effective cohesion  $c'$  and the hydrological properties required by TRIGRS-unsaturated. Due to the connections between all the hydrological properties of the soil, the sensitivity analysis was made to simultaneously change

all these features. For the  $c'$  parameter, the minimum value was set to 0 kPa. The soil hydraulic diffusivity  $D_0$  was estimated based on the characteristic  $K_s$  values of each class, in agreement with Baum et al. (2011) to be  $\sim 2 \times K_s$  (Table 5).

The parameter indicated as  $\alpha_G$  corresponds to the fitting parameter of Gardner's (1958) model for the SWCC. The parameter  $\alpha_G$  was estimated based on the  $\alpha$  and  $n$  fitting parameters of Van Genuchten's model, as reconstructed for each unit through the method proposed by Ghezzehei et al. (2007) and expressed in Eq. (2):

**Table 5.** Mean and standard deviation (SD) values of the soil parameters used as input data in TRIGRS-unsaturated. The SD values are in parentheses.

	$\gamma$ ( $\text{kN m}^{-3}$ )	$\varphi'$ ( $^\circ$ )	$c'$ (kPa)	$\theta_s$ (%)	$\theta_r$ (%)	$\alpha_G$ ( $\text{kPa}^{-1}$ )	$K_s$ ( $\text{m s}^{-1}$ )	$D_0$ ( $\text{m s}^{-1}$ )
Geological unit								
Monte Arzolo Sandstones (SD)	17.9 (1.2)	26 (4)	1.9 (1.1)	44 (5)	6 (5)	0.012 (0.010)	$1.5 \times 10^{-6}$ ( $0.5 \times 10^{-6}$ )	$3.0 \times 10^{-6}$ ( $1 \times 10^{-6}$ )
Rocca Ticozzi Conglomerates (SD)	17.7 (1.5)	27 (4)	1.5 (3.5)	43 (7)	5 (4)	0.012 (0.010)	$1.5 \times 10^{-6}$ ( $0.5 \times 10^{-6}$ )	$3.0 \times 10^{-6}$ ( $1 \times 10^{-6}$ )
Sant'Agata Fossili Marls (SD)	18.0 (1.5)	26 (4)	2.0 (3.0)	46 (5)	8 (6)	0.014 (0.012)	$1.4 \times 10^{-6}$ ( $0.6 \times 10^{-6}$ )	$2.8 \times 10^{-6}$ ( $1 \times 10^{-6}$ )
Gessoso– Solfifera Formation (SD)	17.8 (0.8)	24 (3)	1.8 (3.0)	48 (4)	8 (7)	0.019 (0.013)	$1.4 \times 10^{-6}$ ( $0.5 \times 10^{-6}$ )	$2.8 \times 10^{-6}$ ( $1 \times 10^{-6}$ )
Pedological unit								
BRS1 (SD)	17.0 (1.1)	24 (6)	1.2 (1.2)	46 (4)	7 (6)	0.014 (0.011)	$1.5 \times 10^{-6}$ ( $0.5 \times 10^{-6}$ )	$3.0 \times 10^{-6}$ ( $1 \times 10^{-6}$ )
FGE1 (SD)	17.5 (1.2)	26 (2)	2.0 (3.0)	49 (7)	9 (5)	0.022 (0.018)	$1.5 \times 10^{-6}$ ( $0.5 \times 10^{-6}$ )	$3.0 \times 10^{-6}$ ( $1 \times 10^{-6}$ )
ILM1/RUM1 (SD)	18.1 (1.2)	26 (4)	1.5 (4.2)	43 (4)	5 (5)	0.012 (0.010)	$1.4 \times 10^{-6}$ ( $0.5 \times 10^{-6}$ )	$2.8 \times 10^{-6}$ ( $1 \times 10^{-6}$ )
MRL1 (SD)	18.1 (1.5)	25 (3)	1.5 (3.4)	45 (5)	8 (6)	0.012 (0.009)	$1.4 \times 10^{-6}$ ( $0.5 \times 10^{-6}$ )	$2.8 \times 10^{-6}$ ( $1 \times 10^{-6}$ )

$$\alpha_G = \alpha(1.3n). \quad (2)$$

The slope angle and flow direction maps required by the TopoIndex (Topographic Index) utility were derived from the considered DEM using SAGA Gis (version 2.0.8; Conrad, 2006). By assuming that the gradient of the slope angle is rather uniform along each hillslope on the study area and almost regular – slightly convex in shape – a slope proportional weighting factor (exponent = 1 in TopoIndex) was chosen for the runoff distribution. This scheme distributes the flow excess to all adjacent downslope cells with a weighting factor proportional to the slope (Baum et al., 2008).

To create a continuous map of topsoil thickness, a geomorphologically indexed model based on the local slope angle, the elevation and the topographic position was used (Zizioli et al., 2013).

An analysis of the reliability of the pore water pressure at different depths as modelled by TRIGRS-unsaturated was performed. For the monitoring station and the most intense rainfall events in the wet periods of the monitored time

span (23–25 March 2013, 30 March 2013, 4–5 April 2013, 20–22 April 2013, 18–20 January 2014 and 28 February–2 March 2014; Table 6), the measured values of the pore water pressure measured between 0.6 and 1.2 m from the ground level were compared to the modelled pore water pressure values using TRIGRS-unsaturated.

For these analyses, the initial water table depth across the study area was chosen according to the information obtained during the monitoring time span in the test-site slope. The most superficial measured pore water pressure values (within 0.6 m of the surface) were considered representative of the hydrological conditions in the selected area and were used to estimate the water table depth according to Eq. (3) (Comegna, 2008):

$$d = \frac{\psi_g}{\gamma_w \cos^2 \beta}, \quad (3)$$

where  $\psi_g$  is the pore water pressure near the ground surface,  $d$  is the water table depth,  $\beta$  is the slope angle and  $\gamma_w$  is the unit weight of water.

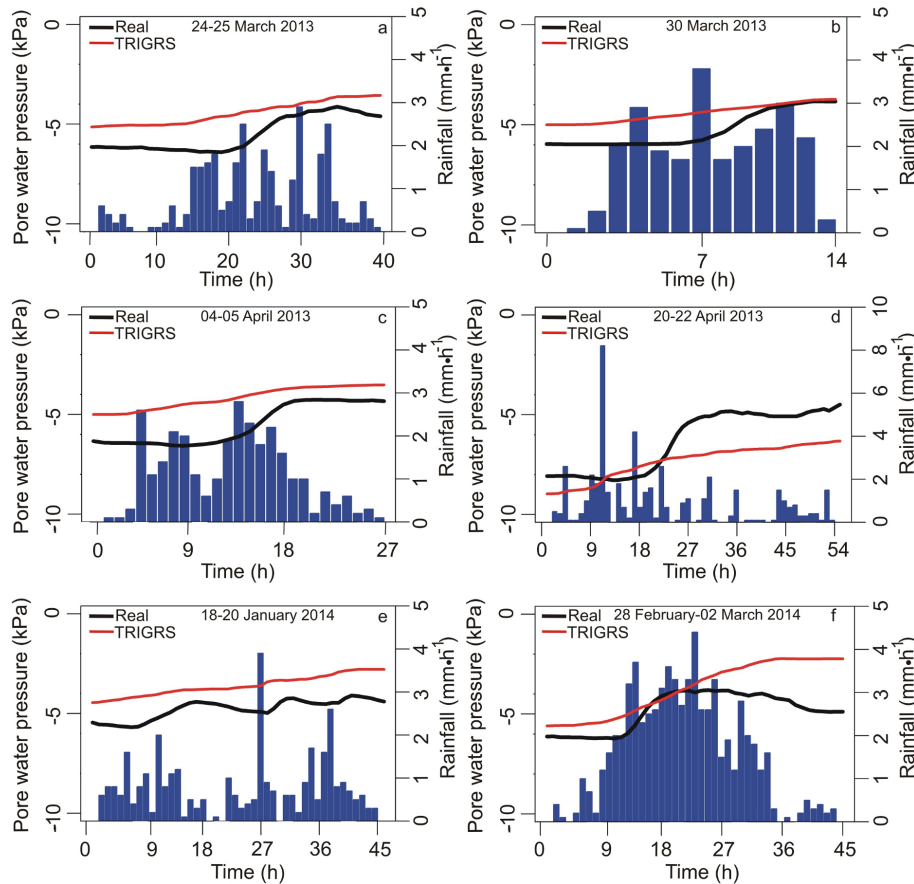


**Figure 9.** Comparison of measured and estimated TRIGRS-unsaturated pore water pressure trends at 0.6 m from ground corresponding to the monitoring station for selected rainfall events: (a) 23–25 March 2013; (b) 30 March 2013; (c) 4–5 April 2013; (d) 20–22 April 2013; (e) 18–20 January 2014; (f) 28 February–2 March 2014.

Hourly values of the data related to the rainfall events from the data logger of the monitoring station were included in the model (Table 6).

The modelling of the pore water pressure for the monitored rainfalls in 2013–2014 was made considering the soil's geotechnical and hydrological data reported in Table 5. In particular, the geological class for the monitoring station area is the Rocca Ticozzi Conglomerates, and the pedological class is ILM1/RUM1.

Moreover, the hourly rainfall intensities recorded by the Cigognola rain gauge during the event that occurred on 27–28 April 2009 were assumed as rainfall input data (Table 6). For these analyses, it was assumed that a thin perched water table was already present in the extended study area before the beginning of the event based on what was observed at the monitoring station during the winters and springs. It was also assumed that this water table had an upper limit located at approximately 0.1 m above the soil–bedrock contact and a parallel trend with respect to this contact.

### 4.3 Comparison between the measured and estimated pore water pressure

Figures 9 and 10 show the comparison between the measured and modelled pore water pressure trends at 0.6 and 1.2 m respectively for the considered rainfall events reported in Table 6. The modelled trends for the test-site soil are the same even when considering the two different mapping unit types because the soil's hydrological properties remain constant (Table 5). Moreover, the same estimated pore water pressure trends were found for the analyses with two different DEMs.

The graphs related to the pore pressure trends show how TRIGRS-unsaturated is able to adequately model the increase in pore pressure during a rainfall event.

In particular, differences greater than 2 kPa between the measured and estimated values have never been found at both depths, except for the final phase of the 28 February–2 March 2014 event. This result can be deemed a very positive result, especially considering that the tensiometers used in the monitoring are characterized by an accuracy equal to  $\pm 1.5$  kPa.

**Table 6.** Selected rainfall events for the implementation of TRIGRS-unsaturated features.

Rainfall event (date time)	Duration (h)	Cumulated rain (mm)	Mean intensity (mm h <sup>-1</sup> )	Minimum intensity (mm h <sup>-1</sup> )	Maximum intensity (mm h <sup>-1</sup> )
26 April 2009, 06:00 LT 28 April 2009, 08:00 LT	62	159.4	2.6	0.0	22.6
23 March 2013, 17:00 LT 25 March 2013, 20:00 LT	40	31.5	0.8	0.1	2.9
30 March 2013, 07:00 LT 30 March 2013, 19:00 LT	13	24.5	1.9	0.1	3.8
4 April 2013, 16:00 LT 5 April 2013, 17:00 LT	26	29.5	1.1	0.1	2.8
20 April 2013, 11:00 LT 22 April 2013, 16:00 LT	54	47.7	0.9	0.0	8.2
18 January 2014, 07:00 LT 20 January 2014, 02:00 LT	44	34.6	0.8	0.0	3.9
28 February 2014, 18:00 LT 2 March 2014, 12:00 LT	43	68.9	1.6	0.0	4.4

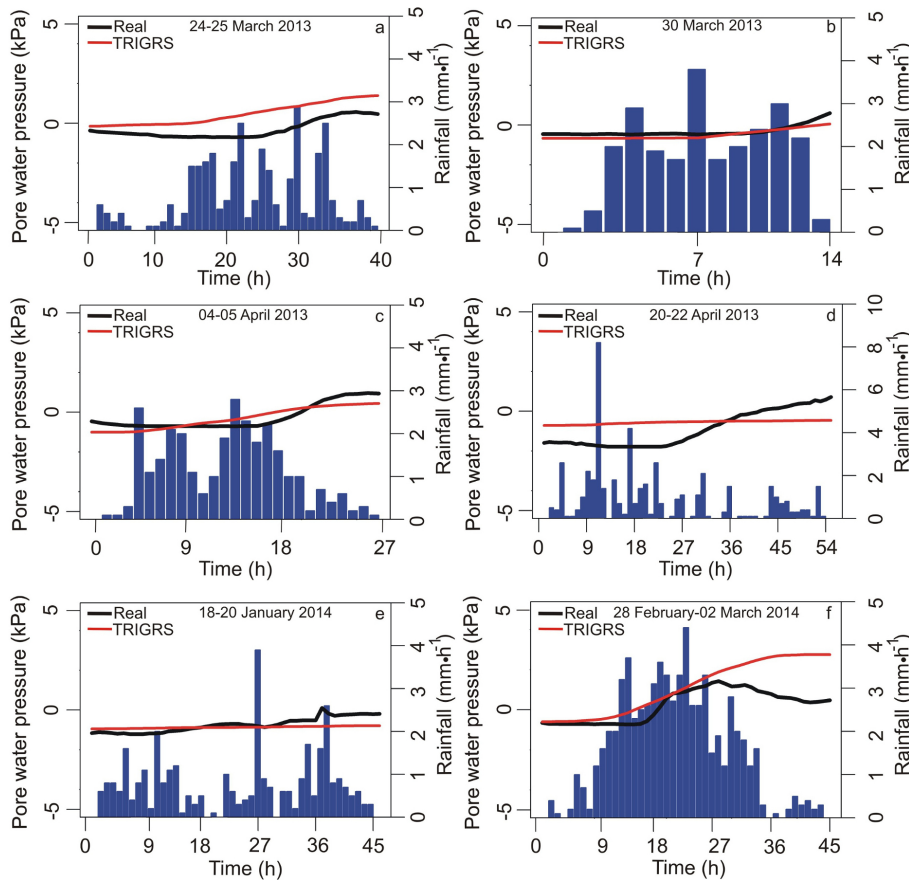


**Figure 10.** Comparison of measured and estimated TRIGRS-unsaturated pore water pressure trends at 1.2 m from ground in correspondence of the monitoring station for selected rainfall events: (a) 23–25 March 2013; (b) 30 March 2013; (c) 4–5 April 2013; (d) 20–22 April 2013; (e) 18–20 January 2014; (f) 28 February–2 March 2014.

**Table 7.** Measured initial–final pore water pressure values versus those computed by TRIGRS-unsaturated for the selected rainfall events at 0.6 m from ground corresponding to the monitoring station in the study area.

Rainfall event (date time)	Initial pore water pressure at –0.6 m (kPa)		Final pore water pressure at –0.6 m (kPa)		RMSE (kPa)
	Meas.	TRIGRS	Meas.	TRIGRS	
23 March 2013, 17:00 LT 25 March 2013, 20:00 LT	–6.1	–5.1	–4.6	–3.6	1.1
30 March 2013, 07:00 LT 30 March 2013, 19:00 LT	–5.9	–5.0	–3.8	–3.7	0.9
4 April 2013, 16:00 LT 5 April 2013, 17:00 LT	–6.3	–5.0	–4.3	–3.5	1.5
20 April 2013, 11:00 LT 22 April 2013, 16:00 LT	–8.1	–9.0	–4.5	–6.3	1.3
18 January 2014, 07:00 LT 20 January 2014, 02:00 LT	–5.5	–4.5	–4.4	–2.8	1.2
28 February 2014, 18:00 LT 2 March 2014, 12:00 LT	–6.1	–5.6	–4.9	–2.2	1.4

**Table 8.** Measured initial–final pore water pressure values versus those computed by TRIGRS-unsaturated for the selected rainfall events at 1.2 m from ground corresponding to the monitoring station in the study area.

Rainfall event (date time)	Initial pore water pressure at –1.2 m (kPa)		Final pore water pressure at –1.2 m (kPa)		RMSE (kPa)
	Meas.	TRIGRS	Meas.	TRIGRS	
23 March 2013, 17:00 LT 25 March 2013, 20:00 LT	–0.4	–0.1	0.5	1.2	0.8
30 March 2013, 07:00 LT 30 March 2013, 19:00 LT	–0.5	–0.6	0.6	0.1	0.2
4 April 2013, 16:00 LT 5 April 2013, 17:00 LT	–0.5	–1.0	–0.9	0.4	0.4
20 April 2013, 11:00 LT 22 April 2013, 16:00 LT	–1.6	–0.7	0.7	–0.4	0.8
18 January 2014, 07:00 LT 20 January 2014, 02:00 LT	–1.2	–0.9	–0.2	–0.8	0.6
28 February 2014, 18:00 LT 2 March 2014, 12:00 LT	–0.7	–0.6	0.5	2.5	1.2

The lowest RMSEs were found for shorter events and depths of 1.2 m compared to those at shallow depths (Table 8). Generally, the RMSEs values are lower than 1.5 kPa for all the considered events and are always lower at 1.2 m from the ground than at 0.6 m (Tables 7 and 8). The differences between the modelled trends at different depths can be linked to the different hydrological properties of the soil horizons. Overall, the increasing pressure trends agree with

each other. The authors of the original code (Baum et al., 2002, 2008) noted that TRIGRS was developed to model intense weather events and not long periods with low levels of precipitation.

Note that a sudden increase in the pore water pressure during the first stages of the rainfall events that occurred on 23–25 March 2013, 30 March 2013 and 4–5 April 2013, as modelled by TRIGRS-unsaturated, is clearly visible at 1.2 m from

the ground (Fig. 10a–c). In particular, the field measurements show a quite negative trend in the pore water pressure, while the model shows a slightly positive trend.

Furthermore, TRIGRS-unsaturated models the highest pore water pressure value at the end of each rainfall event, while in many cases (in particular for the event that occurred on 28 February–2 March 2014) the field measurements show that the highest pore water pressure values are not reached at the end of the event (Figs. 9f and 10f). It is important to note that the  $F_s$  modelled by TRIGRS-unsaturated for these rainfall events always remained over 1.0 (stable conditions). In fact, no shallow landslides were detected after these events next to the monitoring station.

The modelling errors for the pore water pressure trends at the monitoring station can be linked to the simplification provided by the model. The layers within 0.6 m of the surface in the test-site slope soil are somewhat different in terms of the hydrological features with respect to those of the levels between 0.6 and 1.2 m (Table 2). TRIGRS-unsaturated does not consider a layered soil; thus, it is appropriate to simulate the pore water pressure by assuming the mean values of the hydrologic parameters of different layers. Indeed, the mismatch is always lower than 2 kPa, although the mismatch attained a value of 2.8 kPa for the rainfall event on 28 February 2014. It is true that, in general, the variation could have the same range for the mismatch, and then the error could be high with respect to the variation, but we must at least consider the following aspects:

1. the reliability of these results should be evaluated not in an absolute sense, with respect to only isolated rainfall events, but in relation to long-period analyses;
2. during the considered rainfall events, the modelled pore water pressure value is always higher than the measured one; in turn, overestimated pore pressure causes an underestimation of the safety factor of the slope, thus ensuring precautionary conditions;
3. although the results could be considered unsatisfactory at the local scale, the intrinsic limitations of the TRIGRS model (such as the use of a homogeneous soil) together with the extreme potential variation in the hydrologic parameters at the regional scale would make a sensitivity analysis at the local scale inconsistent.

Pore water pressure trends were also modelled for the April 2009 event (Fig. 11), when field measurements were not available and many shallow landslides occurred in the area. For the test-site slope, TRIGRS-unsaturated registered the greatest increase in pore water pressure at 0.6 and 1.2 m around the peak intensities of the event. In particular, the pore water pressure reached approximately 6 kPa at 02:00 LT on 28 April 2009 at 1.2 m and remained constant until the end of the event (Fig. 11). Most landslides were triggered between the late evening of 27 April and the early hours of 28 April (hourly interval 32–48 in the plot of Fig. 11).

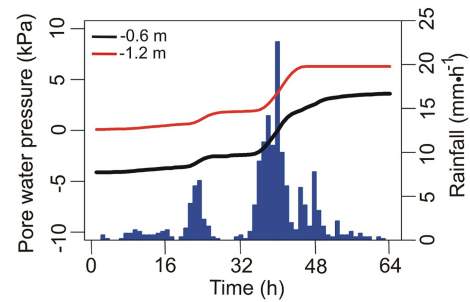


**Figure 11.** Pore water pressure modelled by TRIGRS-unsaturated for 27–28 April 2009 event corresponding to the monitoring station in the study area.

Although a comparison with field measurements is not possible in this case due to the lack of field data, this result can be considered reliable, also accounting for the presence of a perched water table 1.2 m from the ground (positive pore water pressure; Fig. 11) at the beginning of the event, which is also the typical condition observed in the test-site slope during wet months.

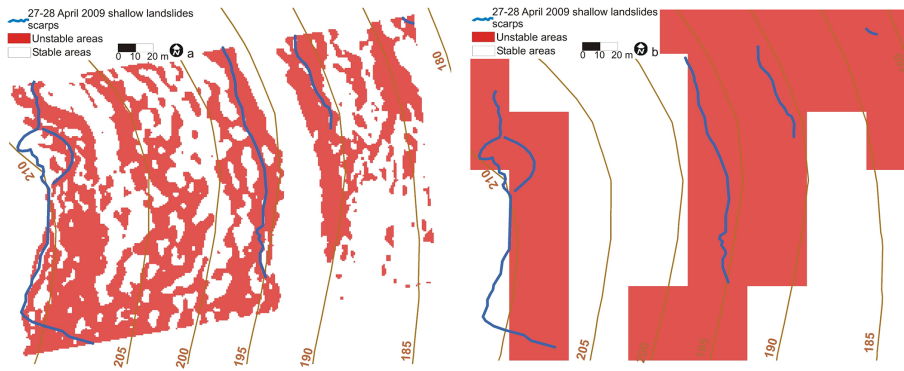
#### 4.4 Identifying shallow landslide triggering zones at different scales

Figure 12 shows the April 2009 scenario at the monitored test-site slope considering DEMs with grid sizes of  $2\text{ m} \times 2\text{ m}$  and of  $10\text{ m} \times 10\text{ m}$ . The figure refers to the period when shallow landslides triggered (between 32 and 48 h since the beginning of the rainfall); after this time span, the scenarios remain steady, following the modelled pore water pressure trend (Fig. 11).

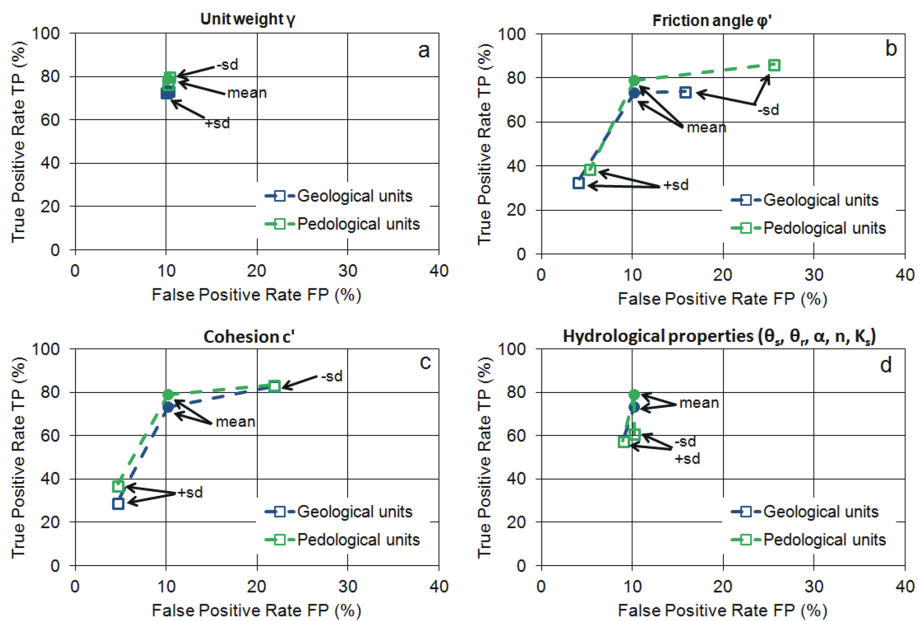
The results were the same when mapping either a geological or pedological zone. In both cases, shallow landslide scarps fell in areas modelled by TRIGRS-unsaturated as unstable (Fig. 12). There is an overestimation of the unstable areas in both the reconstructions because the slope angle is quite steady along the hillslope (between  $25^\circ$  and  $35^\circ$ ). The satisfactory result at the site-specific scale, in terms of the comparison between the modelled and observed landslides, confirms the reliability of the applied methodology.

Figure 13 shows the shallow landslide scenarios for the April 2009 event for the whole study area by taking into account the mean values of the input soil features from the selected mapping unit types. To quantify the differences between the model results based on different mapping units, which also consider the sensitivity analysis, the TP and FP indexes were computed from the  $F_s$  output maps of the study area.

Considering the mean values of the input data, the scenarios based on either geological or pedological units did not provide a significant overestimation of the unstable areas: the maps have similar FP values, ranging between 10.1 and 10.2 % (Fig. 14). The differences between the obtained maps



**Figure 12.** Modelled scenarios for 27–28 April 2009 event for the monitored slope using different DEMs with grid size of 2 m × 2 m (a) and 10 m × 10 m (b).



**Figure 13.** Shallow landslide susceptibility scenarios corresponding to the 27–28 April 2009 event for the study area by using TRIGRS-unsaturated model: (a) geological units and (b) pedological units.

become evident when considering the TP values: the best prediction of the effective unstable areas was obtained considering a pedological mapping unit (78.9 %) with respect to the scenarios obtained through a geological mapping unit, which has a TP index of 73.3 % (Fig. 14).

By analysing the results of the sensitivity analyses, negligible variations in both the TP and FP are linked to the role played by the  $\gamma$  parameter (Fig. 14a), with values on the order of 0.9 and 2.3 % for geological and pedological mapping units respectively. Regarding the hydrological parameters, the best results in terms of the TP are obtained by considering the mean values, with an improvement on the order of 12.3–21.2 % with respect to the values, including the standard deviation. The FP values remain stable in all simulations (Fig. 14d).

Greater variations affect both the TP and FP indexes by changing  $\phi'$  and  $c'$  (Fig. 14b and c). The lowest values of these parameters indicate an improvement in the correct identification of real unstable areas, as indicated by an increase in TP up to 7.3 %, but they also lead to an increase in the areas wrongly mapped as unstable, as indicated by an increase in the FP values up to 37.1 %.

In this case, a nil cohesion value for both pedological mapping units (Fig. 14b and c) has been assumed. The highest values of  $\phi'$  and  $c'$  cause a slight decrease in FP, ranging between 0.2 and 5.7 %, and a significant decrease in TP, ranging between 40.4 and 44.3 % (Fig. 14b and c).

The results obtained through the TRIGRS-unsaturated model have also been compared to the results obtained by Zizioli et al. (2013) for the same area using the TRIGRS-

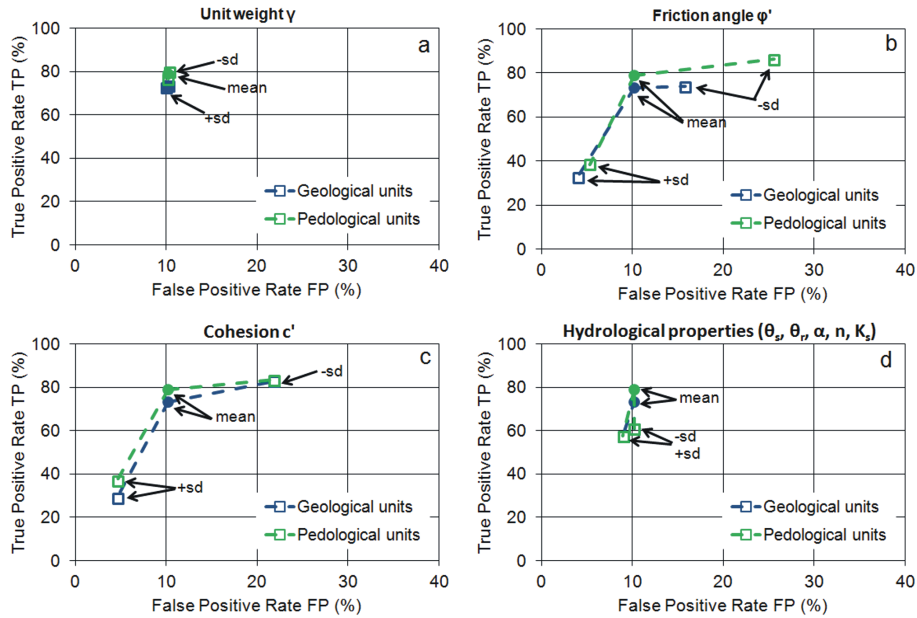


**Figure 14.** Effects of different soil input data on FP and TP indexes obtained by modelling with TRIGRS-unsaturated, considering the values in Table 5 for geological and pedological zoning: (a) unit weight, (b) friction angle, (c) cohesion and (d) hydrological properties.

saturated, SINMAP and SLIP models (Fig. 15). These three models were applied considering different initial hydrological conditions with respect to those considered in this work (Zizioli et al., 2013). Based on the same mapping unit (geological zoning) and considering the mean values of the input soil features, the TRIGRS-unsaturated model provided a better assessment in terms of the ratio between the TP and FP with respect to the other models. In fact, the SLIP and SINMAP models have similar TP (71.7–72.4 %) and FP (30.3–32.2 %), which indicates a significant overestimation of the unstable areas, while TRIGRS-saturated has a lower FP ranging between 10.0 and 10.2 %. The TRIGRS-unsaturated scenario models the effective unstable areas slightly better, as demonstrated by the highest TP value (73.3 %; Fig. 15).

**5 Discussion and conclusions**

In this work, the implementation of a slope stability model for the assessment of the triggering areas of rainfall-induced shallow landslides has been presented. The followed work procedure allowed us to keep the same level of reliability at different scales, both on site-specific slopes and at the local scale for an area some square kilometres wide in the Oltrepò Pavese (northern Italy).

The work procedure consists of the identification of a sample slope in an area of some square kilometres, which can be assumed as representative of the whole area.

Field measurements from a monitoring station installed on the sample slope have previously been analysed. Through monitoring the soil’s hydrological conditions, a detailed de-

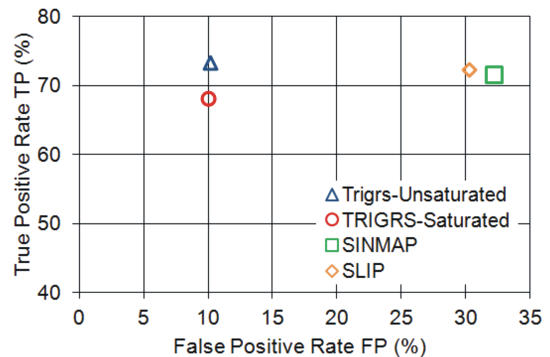


**Figure 15.** True positive rate (TP) and false positive rate (FP) obtained with the TRIGRS-unsaturated, TRIGRS-saturated, SINMAP and SLIP models for the study area considering a geological unit mapping and mean values of soil input data.

scription of the physical–mechanical triggering mechanisms of landslides and the hydrological conditions leading to failure in relation to the site-specific characteristics of the involved soils and stratigraphy has been obtained. In particular, the temporal field measurements of some unsaturated soil hydrological parameters, such as soil water content and pore water pressure, proved of paramount importance. In the study area, the triggering mechanism of rainfall-induced shallow landslides is linked to the emergence of a perched water table present in wet months (winter and spring months) in the slope soils caused by particularly intense rainfalls.

The field measurements also allowed us to adequately verify the reliability of a physically based model for the

identification of shallow landslide triggering zones, which takes into account unsaturated soil conditions such as the TRIGRS-unsaturated model. The assumption according to which the modelled hydrological parameter trends over wide areas should correspond to the real physical processes without an experimental confirmation can cause errors in the assessment of shallow landslide initiation. For this reason, it is necessary to verify the reliability of the model results, even if it necessarily involves only few sample points.

By applying the typical soil hydrological conditions in terms of the perched water table in wetting periods per the field observations, the pore water pressure evaluated by the TRIGRS-unsaturated model essentially agrees with the measurements acquired at the monitored test-site slope for different selected rainfall events.

The correct evaluation of the temporal pore water pressure trend during a rainfall event is fundamental to identify the shallow landslide triggering zones of an area in which the slope soils have incomplete saturation conditions. Based on the good comparison between the measured and modelled pore water pressures for the monitored rainfall events, it was possible to consider the pore water pressure modelled for the 27–28 April 2009 event to be reliable, particularly in terms of the correct discrimination of the increase in pore water pressure due to the intensity peaks during the rainfall.

The site-specific analysis carried out at the test-site slope shows the correct assessment of the shallow landslide scarps from the April 2009 event. Considering DEMs with different resolutions at the scale of the test-site slope, it seems that a higher resolution DEM does not improve the identification of the stable and unstable areas in the sample slope.

After this phase, the same model was applied at the local scale on the surrounding area (13.4 km<sup>2</sup> wide), which had been greatly affected by many shallow landslides in the same event on 27–28 April 2009. Once the reliability of the hydro-mechanical modelling through the TRIGRS-unsaturated model was verified with the improvement linked to the monitored soil hydrological behaviours, it was possible to evaluate the role played by the type of mapping unit on the assessment of unstable areas. Different mapping units (geological and pedological) have been considered, which divided the study area into different classes characterized by a different set of both hydrological and geotechnical soil properties. Furthermore, to take into account the uncertainties linked to the homogenization of the soil input data across the units, a sensitivity analysis was performed to highlight the influence played by each soil feature required by TRIGRS-unsaturated on the assessment of shallow landslide triggering zones.

Considering the mean values of the input data for each unit, the results obtained at the local scale by comparing the real and predicted unstable areas are quite satisfactory in terms of both the true and false positive indexes. The main differences between the models were linked to the TP values of the  $F_s$  maps, while the FP values remained steady at

approximately 10 %, taking into account different mapping (Fig. 14). The best result is obtained by considering a pedological zoning of the study area, which leads to an increase in TP approximately 5 % higher than that obtained by using geological mapping (78.9 and 73.3 % respectively; Fig. 14). The sensitivity analyses showed that the highest influence on the assessment of triggering zones is determined by the change in the soil friction angle and soil cohesion (Fig. 14b and c), especially regarding the overestimation of the unstable areas (significant increase in the FP indexes). A further index useful to evaluate the model's performance is represented by the ratio between the TP and FP. For each mapping unit, the highest ratio between the TP and FP corresponds to the simulation obtained by considering the mean values of the soil input data for all the units. In particular, this ratio is slightly higher for the pedological mapping unit than for the geological one. In addition, the mean values of the soil input data seem to be representative of the units that characterize the study area and seem to attain the best results in all the sensitivity analyses.

Moreover, the results obtained by the TRIGRS-unsaturated model based on the geological units and for the mean values of the input soil data were compared with the results obtained through other physically based models in the same area (Zizioli et al., 2013). The research demonstrates how implementing reliable hydrological conditions derived from the analysis of the typical soil hydrological behaviour and continuous field monitoring improves the prediction of shallow landslide source areas. In fact, based on the same zoning (geological units) of the soil in the study area, the TRIGRS-unsaturated model has a quite higher degree of success with respect to the models (TRIGRS-saturated, SINMAP, SLIP) applied in the past for the same area, which considered different hydrological models and different hydrological input data (Zizioli et al., 2013). The improvement is testified by a significant reduction in the FP on the order of 20 %, which is linked to a lower overestimation of the computed unstable areas. Furthermore, the FP value of the TRIGRS-unsaturated model is higher than that of the other models, thus testifying a better assessment of the shallow landslide triggering areas.

The TRIGRS-unsaturated model results are different, although very close to those previously obtained through the TRIGRS-saturated model (Zizioli et al., 2013). This difference was already shown in other case studies (Sorbino et al., 2010), even if neglecting the effects of the incompletely saturated conditions of the soils can be quite costly on the assessment of shallow landslide triggering zones (Sorbino et al., 2010).

The proposed working scheme for the implementation of the well-established physically based model TRIGRS-unsaturated aims to find a potential methodology for extending the analysis from site-specific to a wider area. An improvement in the results of the model application can be obtained through the use of hydrological monitoring data from

a slope, which can be considered representative of the geomorphological, geological and physical conditions of the surrounding area. In particular, the monitoring approach allows us to identify the typical soil behaviour across different seasons, revealing the response of the slopes to different rainfalls. The monitoring approach is also fundamental for verifying the reliability of a physically based model in terms of the soil's hydrological responses before assessing the triggering zones of shallow landslides. Furthermore, this work gives some indications about the influence of the type of mapping unit chosen for the homogenization of the soil parameters, which are required as input data for the model's application at the local or regional scale. The analysis of the role played by mapping units described in this paper aims to identify which zoning can be more representative of the distribution of the soil's properties over the study area and evaluate the differences in the assessment of triggering areas considering different types of soil mapping units.

The scheme followed in this work can also be applied in other similar contexts to identify slopes prone to shallow landslides and better plan land use. In particular, future developments will be the application of the TRIGRS-unsaturated model in areas affected by shallow landslides and characterized by the extensive presence of slopes cultivated with vineyards, as in Oltrepò Pavese. Furthermore, the role played by wine plant roots on soil reinforcement will be considered, allowing for the development of optimal agricultural management practices to prevent instability phenomena.

### Appendix A: The TRIGRS-unsaturated model

The TRIGRS-unsaturated model (Baum et al., 2008) is a Fortran program designed to model the timing and distribution of rainfall-induced shallow landslides (Baum et al., 2010; Braga et al., 1985; Sorbino et al., 2010; Park et al., 2013; Zizioli et al., 2013). This physically based model considers the method outlined by Iverson (2000) to explain shallow landslide triggering in relation to rainwater infiltration with the implementation of complex storm histories, assuming an impermeable basal boundary at a finite depth and a simple runoff-routing scheme. This model computes the pore water pressure and  $F_s$  during different moments of a rainfall event, which could have durations ranging from hours to a few days, and it identifies, in particular, the changes in the pore water pressure and  $F_s$  due to rainwater infiltration.

The model can consider the unsaturated conditions of the soils at the initial stage through the simple analytic solution for transient unsaturated infiltration proposed by Srivastava and Yeh (1991). The program model's pore water pressure changes using analytical solutions for partial differential equations that represent one-dimensional vertical flow, considering the propagation of the flow into an isotropic, homogeneous material for either saturated or unsaturated conditions according to Iverson's model (Baum et al., 2002, 2008).

To model the soil hydrological pattern for rainwater infiltration, TRIGRS-unsaturated requires soil hydrological properties as input parameters. In particular, in addition to the saturated hydraulic conductivity  $K_s$  and the saturated and residual water contents  $\theta_s$  and  $\theta_r$  respectively, a fitting parameter  $\alpha_G$  that represents the fitting parameter of Gardner's (1958) SWCC fitting equation is required.

The use of step-function series allows TRIGRS-unsaturated to represent pore water pressure changes due to variable rainfall intensity input during the considered event, and a simple runoff-routing model allows for the diversion of excess water from impervious areas to more permeable downslope areas.

An infinite slope model is coupled with the hydrological model to compute the  $F_s$  of a slope. In this case, the  $F_s$  at different time instants at different points and depths in the analysed area ( $F_s(z, t)$ ) is calculated both in unsaturated and saturated conditions, also considering its change over time during the studied rainfall event due to the rise in pore water pressure  $\psi(z, t)$  through Eq. (A1):

$$F_s(z, t) = \frac{\tan \phi'}{\tan \beta} + \frac{c' - \psi(z, t)\gamma_w \tan \phi'}{\gamma z \sin \beta \cos \beta}, \quad (\text{A1})$$

where  $\phi'$  is the soil friction angle,  $c'$  is the effective cohesion,  $\gamma_w$  is the unit weight of the water,  $\beta$  is the slope angle,  $\gamma$  is the unit weight of the soil and  $z$  is the depth below the ground level at which a potential sliding surface could develop.

*Acknowledgements.* We thank M. A. Leoni of the Riccagioia S. C. P. A. – Centro di Ricerca Formazione e Servizi della Vite e del Vino for the pedological analyses of the soil on the monitored slope. We also thank M. Setti of the Department of Earth and Environmental Sciences at the University of Pavia for the X-Ray diffraction analyses of the soil on the monitored slope.

The authors wish to thank the anonymous reviewers for their suggestions and contributions to the work.

Edited by: F. Guzzetti

Reviewed by: two anonymous referees

## References

- Alpert, P., Bengai, T., Baharad, A., Benjamini, Y., Yekutieli, D., Colacino, M., Diodato, L., Ramis, C., Homar, V., Romero, R., Michaelides, S., and Manes, A.: The paradoxical increase of Mediterranean extreme daily rainfall in spite of decrease in total values, *Geophys. Res. Lett.*, 29, 31–1–31–4, doi:10.1029/2001GL013554, 2002.
- Alvioli, M., Guzzetti, F., and Rossi, M.: Scaling properties of rainfall induced landslides predicted by a physically based model, *Geomorphology*, 213, 38–47, doi:10.1016/j.geomorph.2013.12.039, 2014.
- Baum, R. L., Savage, W. Z., and Godt, J. W.: TRIGRS – A FORTRAN Program for Transient Rainfall Infiltration and Grid-Based Regional Slope-Stability Analysis, Open-File Report 02-0424, US Geological Survey, Denver, 35 pp., 2002.
- Baum, R. L., Savage, W. Z., and Godt, J. W.: TRIGRS – A FORTRAN Program for Transient Rainfall Infiltration and Grid-Based Regional Slope-Stability Analysis, version 2.0, Open-File Report 2008-1159, US Geological Survey, Denver, 81 pp., 2008.
- Baum, R. L., Godt, J. W., and Savage, W. Z.: Estimating the timing and location of shallow rainfall-induced landslides using a model for transient, unsaturated infiltration, *J. Geophys. Res.*, 115, F03013, doi:10.1029/2009JF001321, 2010.
- Baum, R. L., Godt, J. W., and Coe, J. A.: Assessing susceptibility and timing of shallow landslide and debris flow initiation in the Oregon Coast Range, USA, in: *Proceedings of the 5th International Conference on Debris Flow Hazards Mitigation, Mechanics, Prediction and Assessment*, 14–17 June 2011, Padua, Italy, edited by: Genevois, R., Hamilton, D. L., and Prestininzi, A., 825–834, 2011.
- Baumhardt, R. L. and Lascano, R. J.: Physical and hydraulic properties of a calcic horizon, *Soil Sci.*, 155, 368–375, 1993.
- Bittelli, M., Valentino, R., Salvatorelli, F., and Rossi Pisa, P.: Monitoring soil-water and displacement conditions leading to landslide occurrence in partially saturated clays, *Geomorphology*, 173–174, 161–173, 2012.
- Bordoni, M., Meisina, C., Zizioli, D., Valentino, R., Bittelli, M., and Chersich, S.: Rainfall-Induced Landslides: Slope Stability Analysis Through Field Monitoring, in: *Landslide science for a safer geoenvironment*, Vol. 3, edited by: Sassa, K., Canuti, P., and Yin, Y., Springer International Publishing, Heidelberg, 273–279, 2014.
- Braga, G., Braschi, G., Calculli, S., Caucia, F., Cerro, A., Colleselli, F., Grisolia, M., Piccio, A., Rossetti, R., Setti, M., Soggetti, F., and Veniale, F.: I fenomeni franosi nell’Oltrepo Pavese: tipologia e cause, *Geologia Applicata e Idrogeologia*, 20, 621–666, 1985.
- Brönnimann, C., Stahli, M., Schneider, P., Seward, L., and Springman S. M.: Bedrock exfiltration as a triggering mechanism for shallow landslides, *Water Resour. Res.*, 49, 5155–5167, doi:10.1002/wrcr.20386, 2013.
- Campus, S., Forlati, F., Susella, G., and Tamberlani, F.: Frane per mobilitazione delle coperture detritiche. in: *Eventi alluvionali in Piemonte, Regione Piemonte, Turin*, 266–287, 1998.
- Comegna, L.: Regional analysis of rainfall-induced landslides. The case of Camaldoli hill, Naples: test case nr. 1 – October, 2004; test case nr. 2 – September, 2005, *Centro euro-Mediterraneo per i Cambiamenti Climatici CMCC, Lecce*, 32 pp., 2008.
- Conrad, O.: SAGA – program structure and current state of implementation, in: *SAGA – Analysis and Modelling Applications*, edited by: Böhner, J., McCloy, K. R., and Strobl, J., *Göttinger Geographische Abhandlungen, Göttingen*, 39–52, 2006.
- Corominas, J., Van Westen, C., Frattini, P., Cascini, L., Malet, J. P., Fotopoulou, S., Catani, F., Van Den Eeckhaut, M., Mavrouli, O., Agliardi, F., Pitilakis, K., Winter, M. G., Pastor, M., Ferlisi, S., Tofani, V., Hervás, J., and Smith, J. T.: Recommendations for the quantitative analysis of landslide risk, *Bull. Eng. Geol. Environ.*, 73, 209–263, 2014.
- Crosta, G. B. and Frattini, P.: Distributed modelling of shallow landslides triggered by intense rainfall, *Nat. Hazards Earth Syst. Sci.*, 3, 81–93, doi:10.5194/nhess-3-81-2003, 2003.
- Cruden, D. M. and Varnes, D. J.: Landslide types and processes, in: *Landslides: investigation and mitigation*, edited by: Turner, A. K. and Schuster, R. L., National Academy Press, Washington, D.C., 36–75, 1996.
- D’Amato Avanzi, G., Giannecchini, R., and Puccinelli, A.: The influence of the geological and geomorphological settings on shallow landslides. An example in a temperate climate environment: the June 19, 1996 event in northwestern Tuscany (Italy), *Eng. Geol.*, 73, 215–228, 2003.
- Damiano, E., Olivares, L., and Picarelli, L.: Steep-slope monitoring in unsaturated pyroclastic soils, *Eng. Geol.*, 137–138, 1–12, 2012.
- Dapporto, S., Aleotti, P., Casagli, N., and Polloni, G.: Analysis of shallow failures triggered by the 14–16 November 2002 event in the Albaredo valley, Valtellina (Northern Italy), *Adv. Geosci.*, 2, 305–308, doi:10.5194/ageo-2-305-2005, 2005.
- ERSAL: I suoli dell’Oltrepo Pavese, Milan, 2001.
- Galve, J. P., Cevasco, A., Brandolini, P., and Soldati, M.: Assessment of shallow landslide risk mitigation measures based on land use planning through probabilistic modelling, *Landslides*, 12, 101–114, doi:10.1007/s10346-014-0478-9, 2015.
- Gardner, W. R.: Some steady-state solutions of the unsaturated moisture flow equation with application to evaporation from a water table, *Soil Sci.*, 85, 228–232, 1958.
- Ghezzehei, T. A., Kneafsey, T. J., and Su, G. W.: Correspondence of the Gardner and van Genuchten/Mualem relative permeability function parameters, *Water Resour. Res.*, 43, 10, W10417, doi:10.1029/2006WR005339, 2007.
- Godt, J. W., Baum, R. L., Savage, W. Z., Salciarini, D., Schulz, W. H., and Harp, E. L.: Transient deterministic shallow landslide modelling: Requirements for susceptibility and hazard assessment in a GIS framework, *Eng. Geol.*, 102, 214–226, 2008a.

- Godt, J. W., Schulz, W. H., Baum, R. L., and Savage, W. Z.: Modelling rainfall conditions for shallow landsliding in Seattle, Washington, in: *Landslides and Engineering Geology of the Seattle, Washington, area*, edited by: Baum, R. L., Godt, J. W., and Highland, L. M., The Geological Society of America, Boulder, 137–152, 2008b.
- Godt, J. W., Baum, R. L., and Lu, N.: Landsliding in partially saturated materials, *Geophys. Res. Lett.*, 36, L02403, doi:10.1029/2008GL035996, 2009.
- Grelle, G., Soriano, M., Revellino, P., Guerriero, L., Anderson, M. G., Diambra, A., Fiorillo, F., Esposito, L., Diodato, N., and Guadagno, F. M.: Space–time prediction of rainfall-induced shallow landslides through a combined probabilistic/deterministic approach, optimized for initial water table conditions, *Bull. Eng. Geol. Environ.*, 73, 877–890, doi:10.1007/s10064-013-0546-8, 2014.
- Hosmer, D. W. and Lemeshow, S.: *Applied logistic regression*, Wiley, New York, 2000.
- Howard, T. R., Baldwin, J. E., and Donley, H. E.: Landslides in Pacifica California, caused by the Storm, in: *Landslides, Floods and Marine Effects of the Storm of January 3–5 1982 in the San Francisco Bay Region, California*, US Geological Survey Professional Paper 1434, edited by: Ellen, S. D. and Wieckzoreck, G. F., US Geological Survey, Denver, 163–184, 1988.
- Iverson, R. M.: Landslide triggering by rain infiltration, *Water Resour. Res.*, 36, 1897–1910, 2000.
- Lanni, C., Borga, M., Rigon, R., and Tarolli, P.: Modelling shallow landslide susceptibility by means of a subsurface flow path connectivity index and estimates of soil depth spatial distribution, *Hydrol. Earth Syst. Sci.*, 16, 3959–3971, doi:10.5194/hess-16-3959-2012, 2012.
- Lim, T. T., Rahardjo, H., Chang, M. F., and Fredlund, D. G.: Effect of rainfall on matric suctions in a residual soil slope, *Can. Geotech. J.*, 33, 618–628, 1996.
- Marquardt, D. W.: An algorithm for least-squares estimation of non-linear parameters, *J. Soc. Ind. Appl. Math.*, 11, 431–441, 1963.
- Matsushi, Y. and Matsukura, Y.: Rainfall thresholds for shallow landsliding derived from pressure-head monitoring: cases with permeable and impermeable bedrocks in Boso Peninsula, Japan, *Earth Surf. Proc. Land.*, 32, 1308–1322, doi:10.1002/esp.1491, 2007.
- Matsushi, Y., Hattaji, T., and Matsukura, Y.: Mechanisms of shallow landslides on soil-mantled hillslopes with permeable and impermeable bedrocks in the Boso Peninsula, Japan, *Geomorphology*, 76, 92–108, doi:10.1016/j.geomorph.2005.10.003, 2006.
- Meisina, C.: Characterisation of weathered clayey soils responsible for shallow landslides, *Nat. Hazards Earth Syst. Sci.*, 6, 825–838, doi:10.5194/nhess-6-825-2006, 2006.
- Meisina, C. and Scarabelli, S.: A comparative analysis of terrain stability models for predicting shallow landslides in colluvial soils, *Geomorphology*, 87, 207–223, 2007.
- Mergili, M., Marchesini, I., Alvioli, M., Metz, M., Schneider-Muntau, B., Rossi, M., and Guzzetti, F.: A strategy for GIS-based 3-D slope stability modelling over large areas, *Geosci. Model Dev.*, 7, 2969–2982, doi:10.5194/gmd-7-2969-2014, 2014.
- Montgomery, D. R. and Dietrich, W. E.: A physically based model for the topographic control on shallow landsliding, *Water Resour. Res.*, 30, 1153–1171, 1994.
- Montrasio, L. and Valentino, R.: A model for triggering mechanisms of shallow landslides, *Nat. Hazards Earth Syst. Sci.*, 8, 1149–1159, doi:10.5194/nhess-8-1149-2008, 2008.
- Mualem, Y.: A new model predicting the hydraulic conductivity of unsaturated porous media, *Water Resour. Res.*, 12, 513–522, 1976.
- Pack, R. T., Tarboton, D. G., and Goodwin, C. G.: SINMAP 2.0 – A Stability Index Approach to Terrain Stability Hazard Mapping, User’s Manual. Produced in ArcView Avenue and C++ for Forest Renewal B. C. under Research Contract No: PA97537-0RE, available at: <http://www.neng.usu.edu/cee/faculty/dtarbot/sinmap.pdf> (last access: 10 December 2014), 1999.
- Papa, M. N., Medina, V., Ciervo, F., and Bateman, A.: Derivation of critical rainfall thresholds for shallow landslides as a tool for debris flow early warning systems, *Hydrol. Earth Syst. Sci.*, 17, 4095–4107, doi:10.5194/hess-17-4095-2013, 2013.
- Park, D. W., Nikhil, N. V., and Lee, S. R.: Landslide and debris flow susceptibility zonation using TRIGRS for the 2011 Seoul landslide event, *Nat. Hazards Earth Syst. Sci.*, 13, 2833–2849, doi:10.5194/nhess-13-2833-2013, 2013.
- Peters, A. and Durner, W.: Simplified evaporation method for determining soil hydraulic properties, *J. Hydrol.*, 356, 147–162, 2008.
- Raia, S., Alvioli, M., Rossi, M., Baum, R. L., Godt, J. W., and Guzzetti, F.: Improving predictive power of physically based rainfall-induced shallow landslide models: a probabilistic approach, *Geosci. Model Dev.*, 7, 495–514, doi:10.5194/gmd-7-495-2014, 2014.
- Rawlins, S. L. and Campbell, G. S.: Water potential: Thermocouple Psychrometry, in: *Methods of Soil Analysis Part 1*, 2nd Edn., Agron. Monogr. 9, Soil Science Society of America, Madison, WI, 597–618, 1986.
- Rossi, G., Catani, F., Leoni, L., Segoni, S., and Tofani, V.: HIRESSS: a physically based slope stability simulator for HPC applications, *Nat. Hazards Earth Syst. Sci.*, 13, 151–166, doi:10.5194/nhess-13-151-2013, 2013.
- Salciarini, D., Godt, J. W., Savage, W. Z., Conversini, R., Baum, R. L., and Michael, J. A.: Modelling regional initiation of rainfall-induced shallow landslides in the eastern Umbria Region of central Italy, *Landslides*, 3, 181–194, 2006.
- Salciarini, D., Godt, J. W., Savage, W. Z., Baum, R. L., and Conversini, R.: Modelling landslide recurrence in Seattle, Washington, USA, *Eng. Geol.*, 102, 227–237, 2008.
- Schaap, M. G., Feike, L. J., and Van Genuchten, M. T.: ROSETTA: a computer program for estimating soil hydraulic parameters with hierarchical pedotransfers functions, *J. Hydrol.*, 251, 163–176, 2001.
- Schindler, U.: Ein schnellverfahren zur messung der wasserleitfähigkeit im teilgesättigten boden an stechzylinderproben, *Arch. Acker-Pflanzenbau Bodenkd.*, 24, 1–7, 1980.
- Schnellmann, R., Busslinger, M., Schneider, H. R., and Rahardjo, H.: Effect of rising water table in an unsaturated slope, *Eng. Geol.*, 114, 71–83, 2010.
- Simoni, S., Zanotti, F., Bertoldi, G., and Rigon, R.: Modelling the probability of occurrence of shallow landslides and channelized debris flows using GEOtop-FS, *Hydrol. Process.*, 22, 532–545, doi:10.1002/hyp.6886, 2008.
- Smethurst, J. A., Clarke, D., and Powrie, W.: Factors controlling the seasonal variation in soil water content and pore water pres-

- tures within a lightly vegetated clay slope, *Geotechnique*, 62, 429–446, doi:10.1680/geot.10.P.097, 2012.
- Sorbino, G., Sica, C., and Cascini, L.: Susceptibility analysis of shallow landslides source areas using physically based models, *Nat. Hazards*, 53, 313–332, 2010.
- Springman, S. M., Thielen, A., Kienzler, P., and Friedel, S.: A long-term field study for the investigation of rainfall-induced landslides, *Geotechnique*, 14, 1177–1193, 2013.
- Srivastava, R. and Yeh, T.-C. J.: Analytical solutions for one-dimensional, transient infiltration toward the water table in homogeneous and layered soils, *Water Resour. Res.*, 27, 753–762, 1991.
- Tiranti, D. and Rabuffetti, D.: Estimation of rainfall thresholds triggering shallow landslides for an operational warning system implementation, *Landslides*, 7, 471–481, 2010.
- Vanapalli, S. K., Fredlund, D. G., Pufahl, D. E., and Clifton, A. W.: Model for the prediction of shear strength with respect to soil suction, *Can. Geotech. J.*, 33, 379–392, 1996.
- Van Genuchten, M. T.: A closed-form equation for predicting the hydraulic conductivity of unsaturated soils, *Soil Sci. Soc. Am. J.*, 44, 892–898, 1980.
- Vercesi, P. and Scagni, G.: Osservazioni sui depositi conglomeratici dello sperone collinare di Stradella, *Rendiconti della Società Geologica Italiana*, 7, 23–26, 1984.
- Zhan, T. L. T., Ng, C. W. W., and Fredlund, D. G.: Instrumentation of an unsaturated expansive soil slope, *Geotech. Test J.*, 30, 1–11, 2006.
- Zizioli, D., Meisina, C., Valentino, R., and Montrasio, L.: Comparison between different approaches to modeling shallow landslide susceptibility: a case history in Oltrepo Pavese, Northern Italy, *Nat. Hazards Earth Syst. Sci.*, 13, 559–573, doi:10.5194/nhess-13-559-2013, 2013.
- Zizioli, D., Meisina, C., Bordoni, M., and Zucca, F.: Rainfall-triggered shallow landslides mapping through Pleiades images, in: *Landslide science for a safer geoenvironment*, vol. 2, edited by: Sassa, K., Canuti, P., and Yin, Y., Springer International Publishing, Heidelberg, 325–329, 2014.